JOINT EUROPEAN TORUS JET

JET–P(91)07

J. Jacquinot, G. Sadler
and JET Team

D-^{3}He Fusion in the JET Tokamak Recent Experimental Results

D-^{3}He Fusion in the JET Tokamak Recent Experimental Results

J. Jacquinot, G. Sadler
and JET Team*

JET-Joint Undertaking, Culham Science Centre, OX14 3DB, Abingdon, UK

** See Appendix 1*

Preprint of Paper to be submitted for publication in
a Special Issue of Fusion Technology on D-^{3}He Fusion

ABSTRACT

A new series of D-^{3}He fusion yield experiments has been performed in JET using ICRF heating to generate a high energy ^{3}He tail reacting with a background Deuterium plasma. Using the recently installed antennas with Beryllium screens, RF power reaching 15 MW could be coupled to the plasma at the fundamental cyclotron resonance of ^{3}He near the magnetic axis. Best results were obtained with 3.5 MA discharges in the double null configuration with high recycling on outboard limiters in order to stay in L mode and to control the plasma density and purity. A record fusion power level of P_{Fus} = 140 kW was obtained, corresponding to a reaction rate of 4.6 10^{16} reactions/s. The amplification factor $Q = P_{Fus}/P_{ICRH}$ reached a maximum of 1.25 % at P_{ICRH} = 10 MW. The previous best results were P_{Fus} = 100 kW and Q = 1 %. Time resolved measurements show a correlation between fusion power and energy stored in the fast ^{3}He ions in agreement with calculations based on classical slowing down of the ^{3}He ions driven by ICRH to an average energy in the MeV range.

I INTRODUCTION

The achievement of high fusion yield from D-^{3}He reactions has been a continuing challenge to Physicists working on fusion plasma research. It certainly constitutes a very severe test of the quality of 3 essential components in a fusion experiment.

a) Confinement. The confinement device must be capable of retaining for several slowing down times (1 - 3 secs) the high energy ions (~ 0.5 MeV) which produce the dominant contribution to the D-^{3}He reaction rate.

b) Heating. The heating method must be capable of producing a substantial ion population with an average energy in the MeV range. This ion population should be located in the plasma centre where it also maintains a high central electron temperature.

c) Measurements. The D-^{3}He reactions must be measured accurately from the very weak branch: D[^{3}He, γ] ^{5}Li despite confusing γ yields originating from nuclear reactions with impurity ions.

Modern tokamaks with currents in excess of 3 MA allow orbits of both the fuel ions (D and ^{3}He) and charged fusion products (^{4}He and H) to be significantly less than the plasma radius and the classical energy decay of these particles is dominated by the slowing down time on electrons.

Heating with powerful waves at the Ion Cyclotron Resonant Frequency (ICRF) is at present the only method available capable of

producing a substantial ion population in the MeV range. All experimental results obtained so far use ICRF at a frequency corresponding closely to the fundamental cyclotron resonance of ^3He ions near the magnetic axis of the tokamak plasma. Only a minority ^3He ion population can be used in order to fulfill simultaneously the following 3 requirements:

1) Sufficient Wave Damping [1] imposes a minimum concentration: $\eta = n_{3_{He}}/n_d \geq 1\ \%$. This condition is not a constraint in the JET experiment

2) Avoidance of Mode Conversion at the D-^{3}He-Hybrid Frequency [1]

$$\eta \leq 1.05 \left[S_{||}\sqrt{\beta_{3_{He}}}\right]^{2/3} \qquad \text{Equation (1)}$$

where $S_{||} = k_{||}c/\omega_{pd}$ is the average normalized wave number of the incident power at the resonance, $\beta_{3_{He}}$ is the kinetic pressure of the minority normalized to the magnetic pressure. ω_{pd} is the deuterium plasma frequency

This condition can be a constraint in the experiment particularly when using the usual "monopole" phasing (in phase launching current straps) which corresponds to a low value of $k_{||}$ (eg $S_{||} \simeq 0.13$ for $n_d = 2.5 \times 10^{19}\ m^{-3}$).

3) Generation of a high energy ^3He tail with "tail temperature" T_t giving the highest reaction rate. Stix's [2] formulation of the anisotropic high energy tail generation gives an optimum ^3He-D reactivity for $T_{t(opt)} \sim 1$ MeV (see appendix and Fig 11).

This condition imposes another constraint on the minority concentration, which can be derived from the Stix result [2]:

$$T_t = T_e (1 + 3 \xi / 2) \qquad \text{Equation 2}$$

with

$$\xi = P\, t_s / (3\, n_{^3He} \cdot kT_e) \qquad \text{Equation 3}$$

or in practical units:

$$\xi = 5.6 \times 10^{37} \frac{P(MW\ m^{-3})\ T_e^{1/2}\ (eV)}{n_e\ m^{-3}\ n_{^3He}\ (m^{-3})} \qquad \text{Equation 4}$$

where P is the RF power density transferred to the ^{3}He ions (typically 60 to 80 % of the input power), t_s is the classical Spitzer ion-electron slowing down time. Combining equations 2 and 3 and assuming $\xi >> 1$, we get the optimum ^{3}He concentration:

$$\left(\frac{n_{^3He}}{n_e}\right)opt = \frac{8.4 \times 10^{31}\ P\ T_e^{3/2}}{n_e^2} \qquad \text{Equation 5}$$

In the appendix, we summarize the calculations of the total D-^{3}He fusion power assuming an anisotropic "Stix" distribution function (eg classical slowing down of the ^{3}He ions) and taking into account the inhomogenities of the plasma parameters and the RF deposition profile. Using the same distribution function, we also calculate the total energy contained in the fast ^{3}He ions driven by ICRF. The results can simply be expressed in the form:

$$P_{fus} = \frac{n_d}{n_e} W_{fast} \cdot \alpha(n_{^3He}/n_e) \qquad \text{Equation 6}$$

$$W_{fast} = \beta\ P_{^3He}\ T_{eo}^{3/2} / n_e \qquad \text{Equation 7}$$

where $P_{^3He} = \int P\, dv$ is the total RF power damped on the ^3He minority. The coefficient α depends mainly on the ^3He concentration and depends only weakly on the other plasma parameters. α goes through a maximum value ($\alpha_{MAX} \simeq 0.1$ to $0.15\ s^{-1}$) when the optimum concentration given by equation 5 is set near the magnetic axis. On the contrary, the coefficient β depends sensitively on the T_e profile and on the RF power deposition profile.

These equations underline the important parameters of the experiments: the central electron temperature needs to be high in order to achieve the required tail temperature, which implies working at low plasma density. The central power density and the plasma purity (n_d/n_e) also need to be high and, finally, the minority density needs to be set to the optimum value. It should be stressed that there exists, at present, no reliable measurement of the ^3He concentration under RF heating in the centre of the JET plasma (the charge exchange recombination measurement is obscured by overlapping beryllium lines) and one can only attempt to obtain the maximum yield by varying the ^3He input flow either with a gas valve, or as done recently in JET for the first time by injecting a 120 keV neutral ^3He beam that they penetrate into the centre.

Experiments on ^3He-D reactivity using the ICRH method have first been reported from the PLT tokamak experiment [4]. Measurements of the unconfined 14.6 MeV protons from the $d[^3He,p]^4He$ reaction enabled estimates of the fusion power to be made which varied in the 0.2 - 1.5 kW range as the applied RF power was increased from 0.4 to 1 MW. The reactivity was estimated within a factor 2 - 3. The central electron temperature was ~ 2 keV.

A series of JET experiments on ^{3}He-D fusion were performed in 1988 [2] with 12 MW of ICRF; the central electron temperature rose to 8 keV and 60 kW of fusion power was generated for about 1 second. The reactivity increased strongly with the coupled RF power - P_{ICRH} - and found to be proportional to $P_{ICRH}^{5/3}$ with some evidence of a weakening of the dependence leading to a saturation in $Q = P_{Fusion}/P_{ICRH}$ at the highest RF power levels. Theoretical estimates of both the perpendicular stored energy associated with the fast ions and the fusion yield agreed with experimental values (with experimental errors of the order of $\simeq$ 20 %) when it was assumed that 65 % of the ICRH power launched by the antenna was coupled to the ^{3}He minority ions (P/P_{ICRH} = 0.65). In these experiments, the central Deuterium concentration was rather low $n_d/n_e \sim 0.3$ due to severe carbon impurity influx.

In a following series of experiments [5], Beryllium evaporation was used as a wall conditioning method and improved central values of n_d/n_e were achieved leading to a higher fusion yield of 100 kW and a global Q of 1 %.

In this paper, we report new experiments performed with beryllium belt limiters and a new set of antenna screens made of beryllium bars reducing the specific RF-induced impurity influx from the screens to a totally negligible level. The experiment also included ^{3}He injection at 120 keV from NBI providing a central source of ^{3}He. Finally, the plasma geometry has been further optimized to allow 5 - 7 second sawtooth-free periods in a 3.5 MA plasma with elongated and triangular cross-section. The central electron temperature now reaches 10 - 12 keV and the maximum fusion yield reaches 140 kW for RF power levels above 10 MW.

The present article presents the experimental method and the results. The results are compared to a simple theoretical analysis based on the standard cyclotron acceleration model and on classical slowing down time.

II EXPERIMENTAL PROCEDURE

The plasma was prepared following the guidance of equations 6 and 7 which requires maximizing P $T_e^{3/2}$ n_d/n_e. On one hand, T_e increases with P_{ICRH}/n_e following approximately an off-set linear law up to a certain value where a saturation occurs, probably due to finite orbit effects on the minority ions [6]. On the other hand, n_d/n_e increases with plasma density (impurity screening effect) and decreases with power. Despite excellent energy confinement, H mode plasmas gave negligible D-^{3}He fusion output because the density rises continuously during the H phase and the electron temperature stays rather low ~ 6 keV; in addition, the H mode phase was short (1.5 to 2 secs) due to carbon influx from the divertor target plate.

JET monster sawtooth discharges have lower energy confinement times than H modes although somewhat better than standard L mode. Typically $\tau_E \sim 1.3\ \tau_E$ (Goldston). The plasma density in these discharges can be controlled by gas puffing under feedback control up to a certain power loading of the limiters. In these experiments, care was taken to minimize the power loading on limiters by shaping the plasma so that it was in contact (see Fig 1) with both the upper divertor target plates (carbon), the belt limiters (beryllium) and the RF antenna side protections (carbon). In a number of cases, the plasma radial position (Fig 3) was swept (±15 mm) using the eigen modes in the RF feedback position system [5]. This method allowed coupling up to 15 MW for several seconds while still controlling the density (2.5 to 3 x 10^{19} m^{-3}) and avoiding excessive impurity contamination. Fig 1a gives the flux contour of the discharge used in the series of experiments reported here; note the points of contacts of the separatrix with both the belt

limiters and the divertor plates. Observations with an infra-red camera confirmed that the exhaust power was shared not only among these elements but also with the side protection tiles of the antenna. Large particle recycling with limiters on the low magnetic field side also serves to prevent a transition to the H mode. Fig 1b gives the flux contours of the discharge used in previous experiments [2,5] which were only in contact with the belt limiters. Note that plasma prepared in the new experimental procedure was far more triangular and elongated.

Fig 2 gives the evolution of the general plasma parameters. Sawteeth are generally not present; a monster sawtooth crash occurs only towards the end of the pulse or even when the RF is ramped down. The sawtooth stabilisation is consistent with the effect of the fast particle population ($W_{fast} \leq 1.5$ MJ, eg about 1/3 of the plasma stored energy). Also apparent in the figure is the fairly good control of electron density. The effective ionic charge Z_{eff} was estimated from charge exchange recombination and from X ray spectroscopy to be Z_{eff} = 2 to 4 depending on the operating sequence.

The ICRF system [7] is made of 8 identical modules. Each amplifier module is driven by an independent frequency source. The frequencies of the 8 sources were chosen to be slightly different from each other in order to reduce cross-talk between antennas due to the presence of toroidal eigen-modes. In the best fusion yield experiments, the 8 frequencies would be regularly spaced between 32 and 33.2 MHz while the vacuum field on the magnetic axis (R = 3.12 m) was set to 2.97 T. The position of the cyclotron resonance of the ^{3}He ions was calculated from the magnetic equilibrium to be R_{res} = 3.02 ±0.05 m.

The resonance was therefore displaced by 0.1 m from the magnetic axis. The spread of frequencies introduces a spread of resonance position by ±0.05 m. Other experiments performed with a different resonance position R_{res} = 3.17 m gave a somewhat lower yield.

Each ICRF module feeds 2 antenna loops which have a toroidal separation of 31 cm between mid-points. In the high power series of the present experiments, the 2 RF loop currents were fed in-phase (monopole configuration) so that the radiated spectrum was rich in low wave number radiation $-3\ m^{-1} < k_{||} < 3\ m^{-1}$. Experiments in the dipole phasing (out of phase) did not exceed a power level of 4 MW due to technical difficulties with the ICRH power plant in this particular series. In all experiments the RF loops were covered by a Faraday screen made of solid beryllium bars inclined by 15° with respect to the horizontal plane, eg nearly aligned with the total magnetic field at the antenna location. The use of beryllium screens reduced to negligible levels the specific impurity generation by the antennas in contrast with previous experiments which used nickel screens [2]. Fig 3 shows the evolution of the frequency and loading resistance of one of the 8 antennas during a high fusion yield experiment. The eigen-modes on the loading resistance shows that the single pass damping is incomplete. Complete damping requires about 3 wave reflections on the outside cut-off surface which matches closely a peripheral magnetic surface. Comparison of the heating efficiency to cases of full damping per pass (H minority) did not reveal any energy loss due to the low damping per pass.

Plasma breakdown occurs in ^3He. Deuterium is injected under feedback control during the entire pulse to maintain the density at the

requested level. ^{3}He could again be injected by gas puffing at the end of the current ramp up phase. In some cases, the JET NBI system was used to inject high energy neutral ^{3}He. However, this procedure did not increase the yield. Table 1 summarizes the conditions of the experiments.

Plasma Current	3.5 MA
Vacuum Toroidal Field (at 2.96 m)	3.1 to 3.45 T
Central Electron Density	2.5 to 3.5 x 10^{19} m^{-3}
Central Electron Temperature	up to 12 keV
Central Ion Temperature	up to 8 keV
Helium 3 Concentration	quite uncertain 1 % to 10 %
ICRF Power (monopole)	up to 15 MW
Frequency	32 to 35.5 MHz
Major Radius of the ^{3}He Cyclotron Resonance (magnetic axis at R = 3.1 m)	3.02 ±.05 m or 3.15 ±0.05 m

TABLE 1
Main Parameters of the High Fusion Experiments

III MEASUREMENT OF THE D-^{3}He REACTION RATE

The fast charged reaction products released in the $^3He + D \rightarrow {}^4He$ (3.7 MeV) + p(14.6 MeV) are well confined in the plasmas ($I_p > 3.5$ MA) considered in this study and even at lower plasma currents the interpretation of measured escaping protons as performed in the pioneering experiments [4] are rendered extremely difficult due to the complicated nature of the orbits followed by these particles. However the γ-rays emitted in the weak secondary branch $^3He + D \rightarrow {}^5Li + \gamma$ (16.6 MeV) are well suited for monitoring the total reaction rate. The detection of these γ-rays requires the use of extremely efficient detectors (intrinsic efficiency = 50 %) and at JET three such detectors are used: a 125 mm x 125 mm long NaI(Tl) scintillator and two 75 mm x 75 mm BGO crystals. Two detectors, the NaI and a BGO, have been used systematically on every discharge since the first successful observations in 1986 [8]. They view the plasma vertically from two well-shielded locations in the roof laboratory and Fig 4 shows their position in relation to the JET machine. The experimental arrangement has been improved from the earlier set-up by the addition of remotely controllable pre-collimators situated on top of the vertical ports of the vacuum vessel and supported by the upper horizontal limbs of the transformer circuit. Also, in expectation of higher γ-ray fluxes, the thickness of neutron filters ($Li_2CO_3 + CH_2$) has been increased and extra Pb γ-ray absorbers installed. The Pb absorbers attenuate the low energy γ-rays preferentially and thus permit higher 16 MeV detection rates. In order to compensate for the narrower line-of-sight imposed by the precollimators, a horizontal line of sight was also installed. This is still under commissioning and, as far as the present study is concerned, has only been used occasionally for checking the volume

integration of the emission as deduced from the NaI detector. The calibration procedure has been described in ref [8] and at the present time the total absolute error is estimated to be less than 30 %.

In the presence of beryllium as the major plasma impurity, the fast ^3He ions undergo highly exothermic reactions with beryllium, releasing energetic neutrons and γ-rays. Neutron yields from these reactions can be sufficiently strong as to compete with the D-D yield and their presence can be easily detected with neutron spectroscopy. Also γ-rays from interactions with Be show up easily on the γ-spectra. If their energy is too high, they start masking the 16 MeV γ-ray emission and many of the discharges from this campaign had to be disregarded because of excessive contamination by Be γ-rays. On several occasions the emission rate from such reactions was so high that an estimate on the power released in these reactions gave 1 - 5 kW.

IV EXPERIMENTAL RESULTS

Most of our experimental data points were obtained in 3.5 MA double null discharges with the wall power loading shared between the upper (carbon), the lower (beryllium) x-point dump plates and the Be belt limiter, as described above. High current discharges ($I_p \geq 4.5$ MA) in JET can only be obtained in the limiter configuration and are therefore likely to have a higher Be contamination preventing a proper analysis of the γ–ray spectra and/or leading to a poorer performance.

The full data-set is shown in Fig 5, giving the 16 MeV γ-ray count-rate as a function of applied RF power. For comparison, a data point from a 5 MA limiter discharge is shown; all the other points refer to 3.5 MA, double null x-point discharges.

First we notice the power dependence of the γ-ray yield as a function of RF power. The exponent 'α' in $N_\gamma \propto P^{\alpha}_{ICRH}$, compatible with the upper bound of the data set, is 1.7 for RF power levels in the range from 3 to 10 MW. In a previous investigation [2] the value of 1.7 was representative of the full data set and not only its upper bound. The large scatter of the data in the present series of experiments is discussed at the end of this section.

Converting count-rates into total γ-ray yields taking into account line-of-sight and absorbers gives a good measure of the generated fusion power. As can be seen in Fig 6 the highest yields achieved approach 140 kW and, therefore, lie substantially above the previous record of 100 kW obtained during the Be gettering phase of the JET experiments in 1989. Above about 10 MW of coupled RF power the

yield seems to saturate, possibly caused by excessive impurity generation and/or an acceleration of the minority ions above their optimal energy. The effect of this saturation can be seen more clearly in Fig 7, where the fusion multiplication factor $Q = P_{Fus}/P_{ICRH}$ is shown as a function of coupled RF power. The maximum of Q is reached at moderate values of the coupled power ($6\ MW < P_{ICRH} < 10\ MW$) and clearly exceeds the previous best values of 1 % from the Be gettering phase and 0.5 % in the pure carbon phase.

As expected from equations 6 and 7, Fig 6 shows a clear correlation between $P_{ICRH}\ T_e^{3/2}/n_e$ and the maximum fusion yield from experiments with variable ^3He concentrations. The behaviour expected from equation 6 is also well demonstrated in Fig 8 which represents time-resolved measurements of W_{fast} (deduced from magnetic measurements) and measured γ-emission rate during a single long plasma pulse.

Finally we present the data base (Fig 9) in the P_{fus} versus W_{fast} plane. The representation removes the scatter (compare Figs 5 and 9) due to variable plasma conditions, in particular the electron temperature profiles. The remaining scatter is thought to reflect a large but not well known variation of the ^3He and D concentration. This result is in agreement with a simple theory (appendix) based on "classical" RF tail formation process and slowing down due to electron drag and ion collisions. In other words, the maximum observed yield of 140 kW also corresponds to the maximum yield which could be achieved for the theoretical optimum concentration (here $n_{^3He}/n_e \cong 0.07$) and for $n_d/n_e \sim 0.5$ to 0.65. Such a value of n_d/n_e is determined experimentally from the absolute D-D reaction rate measurement.

Finally we note that the agreement with theory also constitutes proof that the ^{3}He high energy tail did reach the optimum 1 MeV value.

CONCLUSIONS

In a recent series of experiments to study the fusion reactivity generated between ICRH-driven ^{3}He minority ions and the background deuterons, up to 15 MW of RF power was coupled to the JET plasma giving a measured Q ≈ 1.25 %. The maximum Q value was obtained with 10 MW input power. A maximum fusion yield of 140 kW in charged particle products was reached at a somewhat higher input power of 14 MW.

The maximum fusion yield is approximately proportional to W_{fast} or $P_{ICRH}\ T_e^{3/2}/n_e$ as expected from an elementary theory (equation 6) which neglects orbit effects and anomalous diffusion of the fast particles. This correlation with $W_{fast} = \alpha\ P_{ICRH}\ T_e^{3/2}/n_e$ is found either when comparing different experiments (Fig 9) or during long pulses using time resolved measurements, Fig 8. The scattering of the data points shown in Fig 9 is ascribed to varying concentrations of the Helium 3 and Deuterium since obtaining the maximum yield requires working at the optimum concentration. The observed maximum fusion yield corresponds accurately to the maximum theoretical yield for the observed value of stored energy in the fast particle (W_{fast}). Injecting ^{3}He atoms at 120 keV with the JET NBI system actually lowered the yield, presumably because the ^{3}He concentration exceeded the optimium calculated value of 0.07 in this series.

It is interesting to note the progress made (gain by a factor 2.3) both in Q and P_{fusion} since the first JET experiments [8] which used the same RF power level. Much of this progress results from the replacement of carbon limiters and nickel antenna screens by beryllium limiters and beryllium screens which allow higher values of n_d/n_e for a given value of P/n_e (see for instance Fig 1 of reference 9, which gives an increase of n_d/n_e by a factor 1.3 to 2). However, the change of limiter material is insufficient to explain all the progress made. The plasma prepared for these experiments also had better confinement properties. The plasma current was higher (3.5 MA instead of 3 MA) and the geometry was close to a double null configuration; consequently, the electron temperature was increased and the energy stored in fast particles was higher.

Further progress appears possible in JET by improving W_{fast}, eg increasing the central electron temperature. This may be achieved by working at high current (5 MA) and increasing the central electron power input while maintaining sawtooth-free discharges. The use of higher ICRH power and of the LHCD system recently installed in JET may provide the required additional features.

ACKNOWLEDGEMENT

It is a pleasure to thank our colleagues in the JET team for assistance in this work. Particular thanks go to the tokamak operating teams (Task Forces L and P), to the additional heating groups (ICRH and NBI) and to the members of all the diagnostic groups involved in the measurements reported here.

APPENDIX

In this section, we calculate the observable quantities of the experiments, P_{fus} and W_{fast}, assuming a classical description for the generation of a high energy ^3He tail by fast magnetosonic waves which is balanced by electron drag and by collisions with the main ion species. We use the Stix's formulation [2] of the anisotropic distribution function. Then we calculate various moments of this distribution taking into account the inhomogenities of the plasma parameters. Since, in this work we can only observe moments of the distribution function and not the distribution function itself it is sufficient to use a simple description neglecting contributions from higher order terms [10]. Finite larmor radius effects can be included by implementing a broadening of the RF power deposition profile.

Consider a test ^3He ion energy E in a deuterium plasma. The critical energy for electron drag to dominate ion collisions is:

$$E_{crit} = 14.8\, kT_e \left\{ \frac{A^{3/2}}{n_e} \sum_j \frac{n_j Z_j^2}{A_j} \right\}^{2/3} \qquad \text{Equation 8}$$

where A and A_j are the atomic masses of the test and field ions and kT_e the electron temperature. The summation is taken over the field ions. Taking T_e = 10 keV and $n_e = 3 \times 10^{19}$ cm^{-3} we find:

$$E_{crit} \simeq 300 \text{ keV}$$

Since most of the D-^{3}He fusion reactions take place at about 0.7 MeV, it is legitimate to consider an anisotropic distribution with only 2 degrees of freedom in the direction perpendicular to the confining field on the basis that cyclotron resonance provides perpendicular energy which cannot be isotropized by the electron drag process. A discussion of this result is given by Stix [2] and we use his formulation of the anisotropic distribution of the ^{3}He distribution function f(E) (equation 38 of Reference 2).

We then calculate the local energy density (perpendicular energy) in the fast ions.

$$w_{fast} = 1.6 \times 10^{-19}\, n_{3_{He}} \int_0^\infty F(E) E\, dE \qquad \text{Equation 9}$$

The local D-^{3}He fusion reactivity is given by:

$$\Re = n_D n_{3_{He}} \int_0^\infty F(E) < \sigma v > dE \qquad \text{Equation 10}$$

where $<\sigma v>$ (Fig 10) is calculated with an updated cross-section σ and takes into account collisions between test ^{3}He particles and a maxwellian background deuterium species (T_i = 10 keV).

We now consider an inhomogeneous toroidal plasma with an eliptical cross-section (elipticity in the centre ε = 1.3) and with density profiles matching the experimental data:

$$n_e(r) = n_e\,[1 - r^2/a^2]^{0.5}$$

$$n_{^3He}(r)/n_e(r) = \eta$$

$$\frac{n_d(r)}{n_e(r)} = \frac{Z_{eff} - Z_{imp}}{1 + 4\eta - Z_{imp}(1 + 2\eta)}$$

where $Z_{imp} = 4$ (eg beryllium) and $Z_{eff} = 2$ has been chosen in the calculation.

The temperatures have been modelled with peaked profiles as measured during the experiments:

$$T_e(r) = T_e\,[1 - r^2/a^2]^4$$

$$T_i(r)/T_e(r) = 0.8$$

The RF power density has been given the form:

$$P = P_O \exp\,[-\,r^2/w^2]$$

A value w = 0.35 m has been used in the calculation. It has been derived as a sum of 3 terms,

$$w = w_i + w_r + w_o$$

where W_i is the intrinsic RF power deposition calculated from full wave codes when the resonance passes through the magnetic axis ($W_i \sim 0.15$). W_R describes the off-set of the resonance from the magnetic axis

($W_R \sim 0.1$) and finally W_O is the broadening due to finite orbit size at E $\sim$ 0.7 MeV ($W_O \sim 0.1$).

Finally, we derive the total fusion power output and the total energy in fast particles by integrating equations 9 and 10 over the plasma volume (a is the plasma radius; R is the major radius):

$$W_{fast} = 4\pi^2 R\varepsilon \int_0^a w_{fast}\, rdr \qquad \text{Equation 11}$$

$$P_{fus} = 4\pi^2 R\varepsilon\, 18.3 \times 10^6\, 1.6 \times 10^{-19} \int_0^a \Re\, rdr \qquad \text{Equation 12}$$

Table 2 summarizes the input parameters in the calculations and the most salient results. Fig 11 gives the fusion reactivity in the centre as a function of the ^{3}He concentration. The optimum reactivity in the centre is obtained for $\eta \simeq 0.12$. This optimum concentration varies with the plasma parameters according to equation 5. On the contrary, the optimum tail temperature does not vary much and is always close to 1 MeV. The variation of the fast particle energy density with the concentration is given in Fig 12. The reduction of W_{fast} with η results from the increasing importance of the ion collisionality as the average fast particle energy decreases and approaches E_{crit}. This curve can be used as a guide line in the experiments to find the optimum ^{3}He concentration without making a direct measurement: one should increase the ^{3}He concentration until W_{fast} is reduced by a factor 0.7 from its value at low concentration.

Finally, the result of the volume integration is shown in Fig 13. The optimum fusion output is obtained for a ^3He concentration $\eta \simeq 0.07$ meaning that the central tail temperature must be somewhat overdriven to make the best use of the plasma volume.

Both the total energy content W_{fast} and the total fusion power output agree within 20 % with the observed values (Fig 9) for $n_d/n_e \simeq 0.6$. This is a strong indication that there are no large anomalous processes either in the cyclotron acceleration model nor in the confinement of the fast ions for the level of power which has been reached so far. This conclusion agrees with previous JET studies [6].

INPUT IN THE CALCULATIONS	
• Total power transferred to ^3He ions (about 80 % of the total coupled power)	10 MW
• Half width of the gaussian power deposition profile	0.35 m
• Central Electron Temperature	10 keV
• Central Electron Density	2.5×10^{19} m^{-3}
• Z_{eff}	2
• Deuterium concentration n_d/n_e	~ 0.6
OUTPUT FROM THE CALCULATIONS	
• Fusion yield at optimum concentration	126 kW
• Optimum ^3He concentration	0.07
• Optimum high energy tail temperature	1 MeV

TABLE 2
Input Parameters and Output Values in the Calculations

REFERENCES

[1] J. G. Jacquinot and Y. Lapierre, "Damping Mechanisms and Heating Scenarii in the ICRF", Proceeding of the 2nd Joint Grenoble - Varenna International Symposium, Como, Vol 1, p. 541 (1980). See also J. Adam, J. Jacquinot, H Kuus, "Physics Aspects and Technical Elements of an ICRF Heating System for JET", EUR-CEA-FC-1065 (1980).

[2] D. A. Boyd, D. J. Campbell, J. G. Cordey, W. G. Core, J. P. Christiansen, G. A. Cottrell, L. G. Eriksson, T. Hellsten, J. G. Jacquinot, O. N. Jarvis, S. Kissel, C. Lowry, P. Nielsen, G. Sadler, D. F. H. Start, P. R. Thomas, P. Van Belle and J. A. Wesson, "^{3}He-D Fusion Rate Measurements During Fast Wave Heating Experiments in JET, Nucl. Fusion 29(4), 593 (1989). Note the error in the vertical scale of Fig 1 in this paper which should be divided by 10, also the optimum tail temperature should be corrected from 250 keV to 1 MeV, a value found when ion collisionality and the pressure anisotropy is taken into account..

[3] T. H. Stix, Nucl. Fusion 15, 737 (1975).

[4] R. E. Chrien and J. D. Strachan, Phys. Fluids, 26(7), 1953-1964 (1983)

[5] JET Team (presented by D. F. H. Start), "ICRF Heating.in Reactor Grade Plasmas", IAEA-CN-53/E-2-1 (1990).

[6] G. A. Cottrell, D. F. H. Start, "A Large Orbit Model of Fast Ion Slowing Down during ICRH: Comparison with JET Data", Nuclear Fusion, Vol 31, No 1 (1991).

[7] J. G. Jacquinot, V. P. Bhatnagar, H. Brinkschulte, M. Bures, S. Corti, G. A. Cottrell, M. Evrard, D. Gambier, A. S. Kaye, P. Lallia, F. Sand, C Schueller, A. Tanga, K. Thomsen and T. J. Wade, Royal Soc. Lond. A322, 3-15 (1987).

[8] G. Sadler, O. N. Jarvis, P. Van Belle, N. Hawkes and B. Syme in Controlled Fusion and Plasma Heating (Proc 14th European Conference, Madrid, 1987), Vol 11 D, Part 3, European Physical Society (1987) 1232.

[9] The JET Team (presented by P-H Rebut), "Recent JET Results and Future Prospects", IAEA-CN-53/A-1-2 (1990), also JET-P(90)62.

[10] L. G. Eriksson, Private Communication.

FIGURE CAPTIONS

Fig 1: Poloidal flux contours in the plasma used in the series of experiments reported here (Fig 1a) and in a previous series of experiments performed in 1989 (Fib 1b). The points of contact of the last closed surfaces with the limiters are indicated.

Fig 2: Evolution of the important quantities during a typical high fusion yield experiments: plasma current (I_p), ICRF power, NBI ^{3}He for fuelling and D for charge exchange measurements, central electron temperature (T_{eo}) and density (n_{eo}).

Fig 3: Evolution of the ICRF antenna loading resistance (R_c), the antenna-plasma distance and ICRH frequency. Both the antenna-plasma distance and the RF frequency are under feedback control to maintain constant R_c and the imaginary impedance seen by the generators.

Fig: 4 Experimental arrangement showing one of the two vertical lines-of-sight used in the series of experiment described in the present paper.

Fig 5: Variation of γ-ray yield as a function of coupled RF power;
Δ ^{3}He gas puff, monopole configuration, 3.5 MA
$\square$ ^{3}He NBI, monopole configuration, 3.5 MA
$\diamond$ ^{3}He gas puff and/or ^{3}He NBI, dipole configuration, 3.5 MA
O ^{3}He gas puff, monopole configuration, 5 MA

Fig 6: D-^{3}He Fusion Power as a function of $P_{ICRH}\ T_e^{3/2}\ n_e \propto W_{fast}$ for 3.5 MA discharges;
Δ ^{3}He gas puff
□ ^{3}He NBI

Fig 7: Measured Q as a function of coupled RF power for 3.5 MA discharges with the RF antennas in monopole configuration;
Δ ^{3}He gas puff
□ ^{3}He NBI

Fig 8: Time evolution of **a)** D-^{3}He γ-ray emission, **b)** coupled RF power, **c)** central electron temperature, and **d)** perpendicular energy stored in fast particles deduced from magnetic measurements (diamagnetism and plasma equilibrium). Note the correlation between the fusion yield and W_{fast} as predicted by equation 6.

Fig 9: D-^{3}He fusion yield versus the perpendicular energy of the fast ^{3}He ions determined from magnetic measurements ($W_{fast} = 4(W_{dia} - w_{MHD})/3$). These results should be compared to the theoretical results of Fig 13.

Fig 10: $< \sigma v >$ versus ^{3}He test particle energy calculated from updated cross-sections. The calculation is made for test ^{3}He particles colliding on a maxwellian background deuterium species (T_i = 10 keV).

Fig 11: Central values of the fusion reactivity and ^3He tail temperature T_t versus $\eta = n_{^3He}/n_e$. The optimum conditions corresponds to $T_t \sim 1$ MeV and $\eta \sim 0.12$.

Fig 12: Central value of the fast particle energy density versus η.

Fig 13: Total fusion output versus W_{fast} from equations 11 and 12. The ^3He concentration η is indicated on the curves. The parameters are given in Table 2 except for: lower curve, T_e = 8 keV, P = 7.5 MW and upper curve T_e = 10 keV, P = 10 MW.

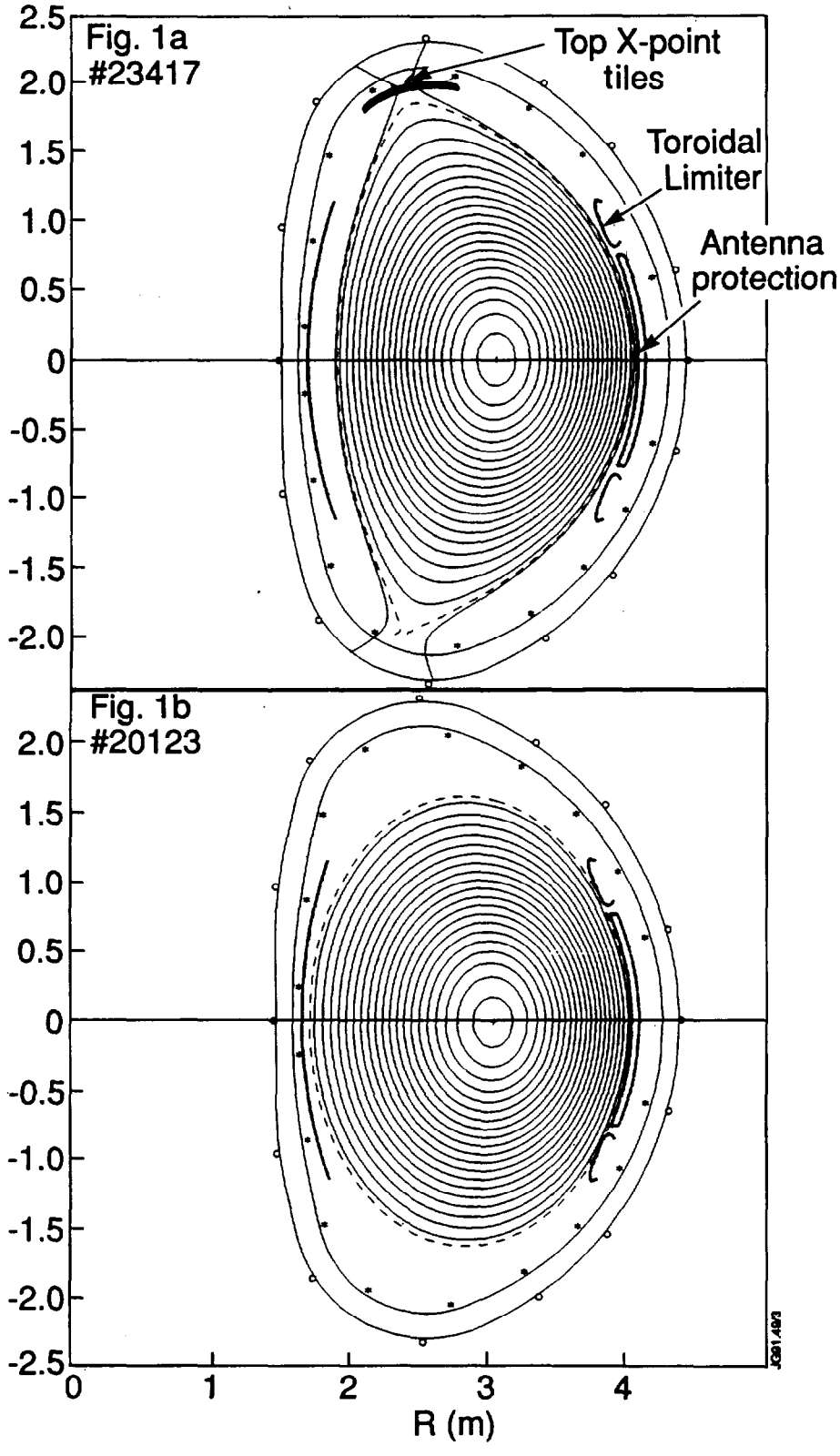

Fig 1: Poloidal flux contours in the plasma used in the series of experiments reported here (Fig 1a) and in a previous series of experiments performed in 1989 (Fib 1b). The points of contact of the last closed surfaces with the limiters are indicated.

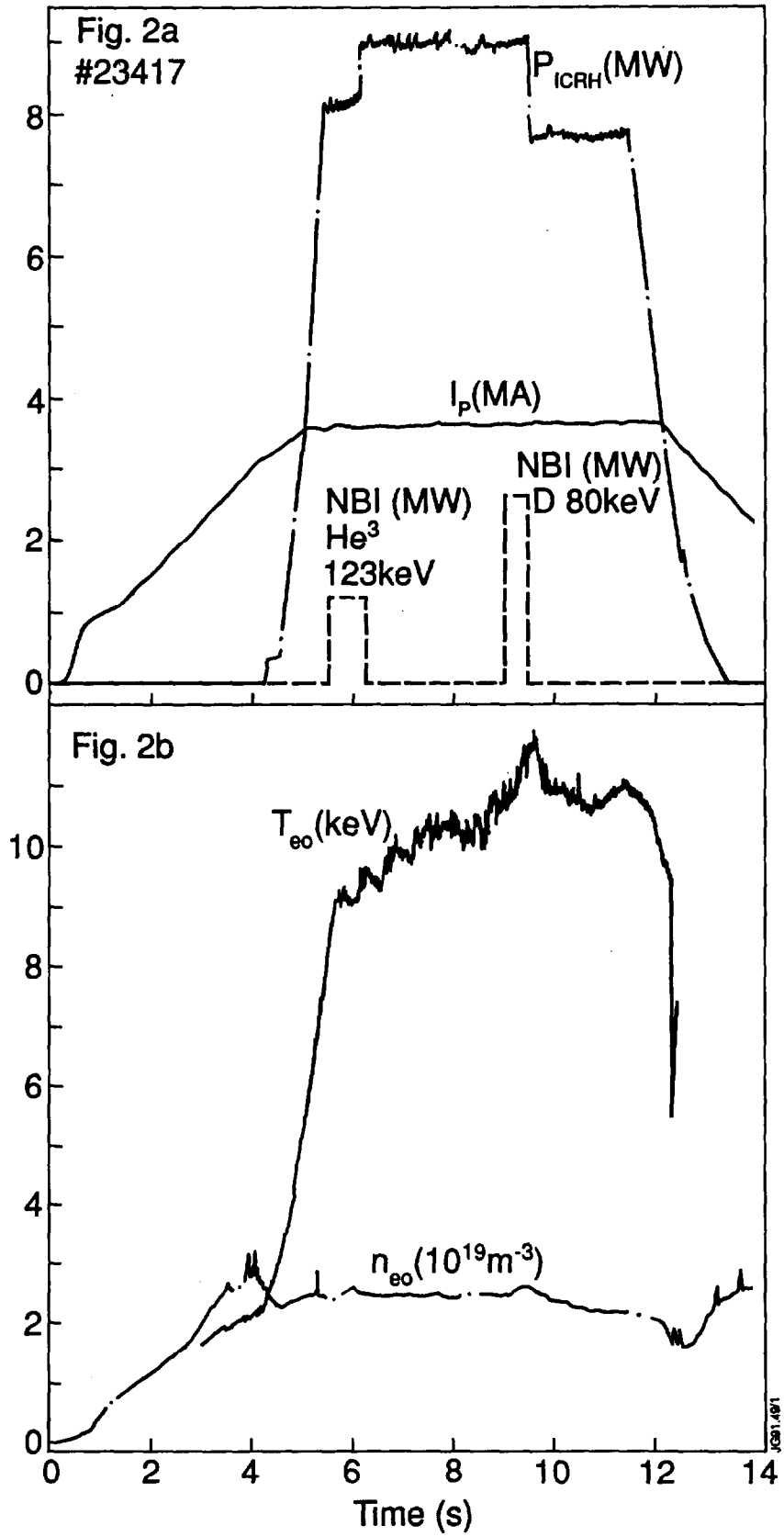

Fig 2: Evolution of the important quantities during a typical high fusion yield experiments: plasma current (I_p), ICRF power, NBI ^{3}He for fuelling and D for charge exchange measurements, central electron temperature (T_{eo}) and density (n_{eo}).

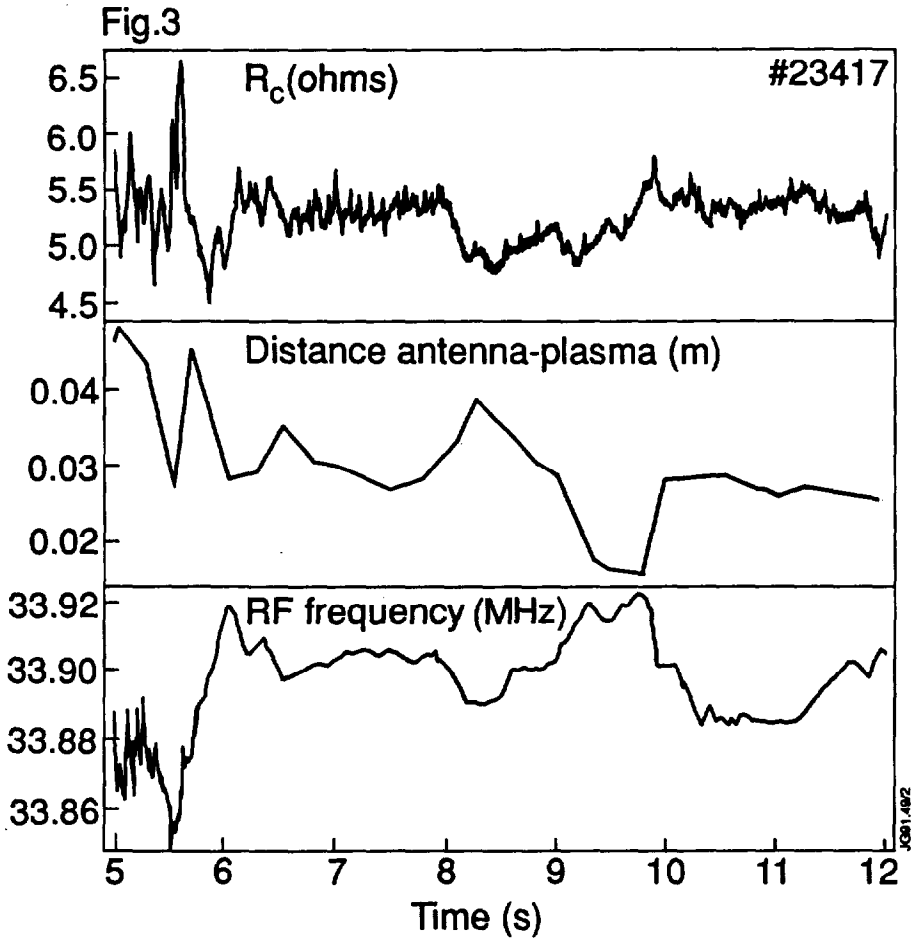

Fig 3: Evolution of the ICRF antenna loading resistance (R_C), the antenna-plasma distance and ICRH frequency. Both the antenna-plasma distance and the RF frequency are under feedback control to maintain constant R_C and the imaginary impedance seen by the generators.

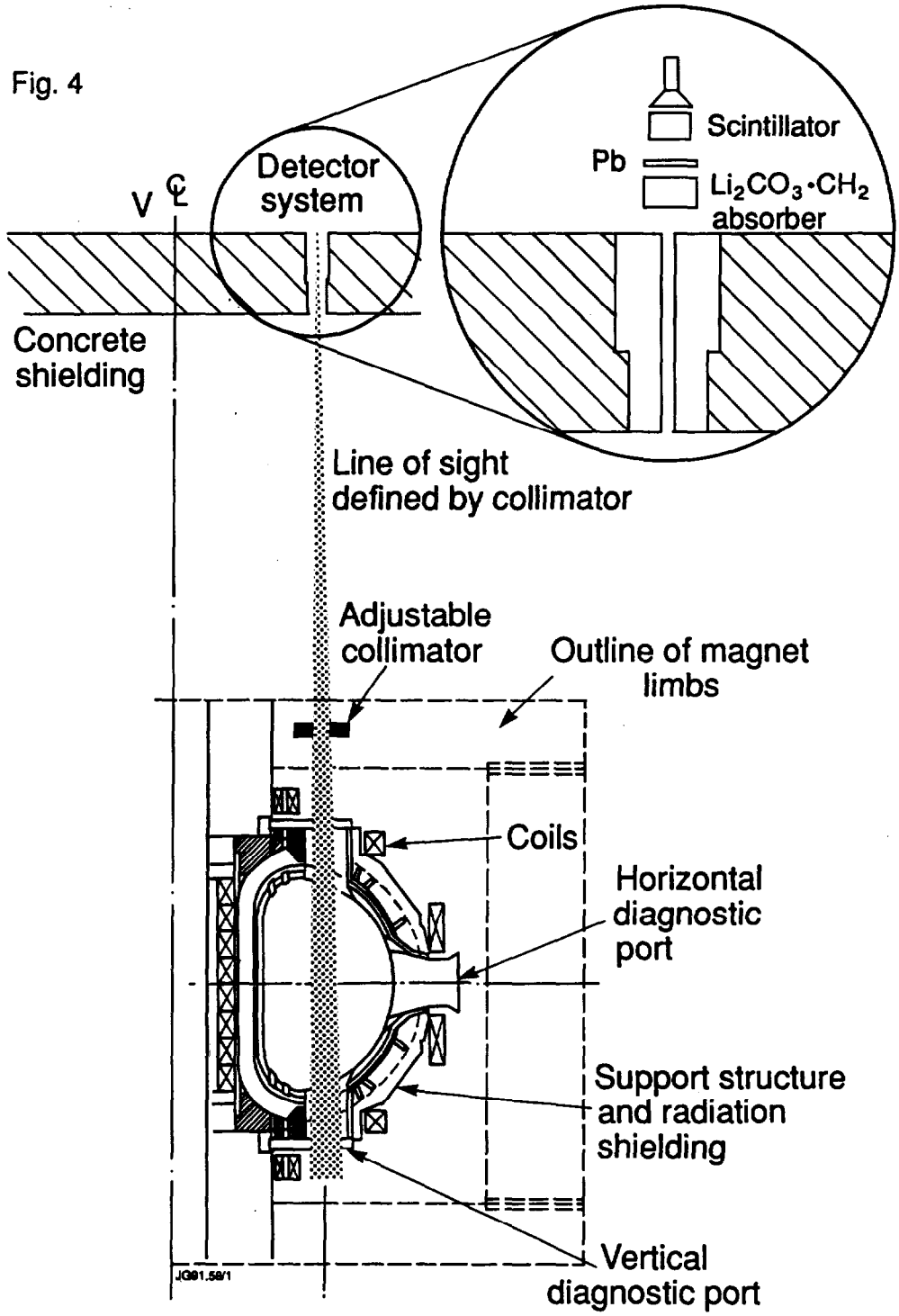

Fig: 4 Experimental arrangement showing one of the two vertical lines-of-sight used in the series of experiment described in the present paper.

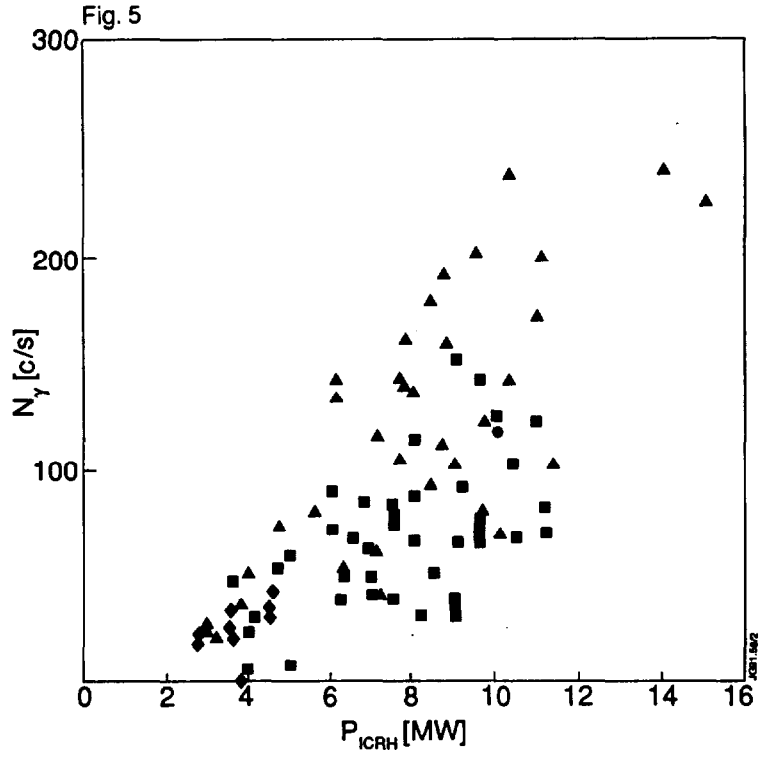

Fig 5: Variation of γ-ray yield as a function of coupled RF power;
▲ ^{3}He gas puff, monopole configuration, 3.5 MA
■ ^{3}He NBI, monopole configuration, 3.5 MA
◆ ^{3}He gas puff and/or ^{3}He NBI, dipole configuration, 3.5 MA
● ^{3}He gas puff, monopole configuration, 5 MA

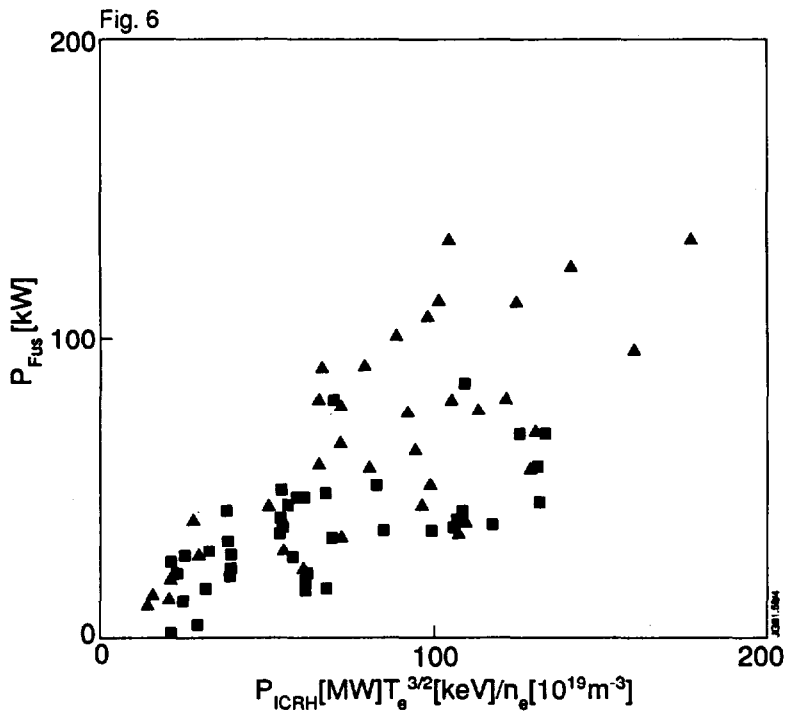

Fig 6: D-^{3}He Fusion Power as a function of $P_{ICRH}\ T_e^{3/2}\ n_e \propto W_{fast}$ for 3.5 MA discharges;
▲ ^{3}He gas puff
■ ^{3}He NBI

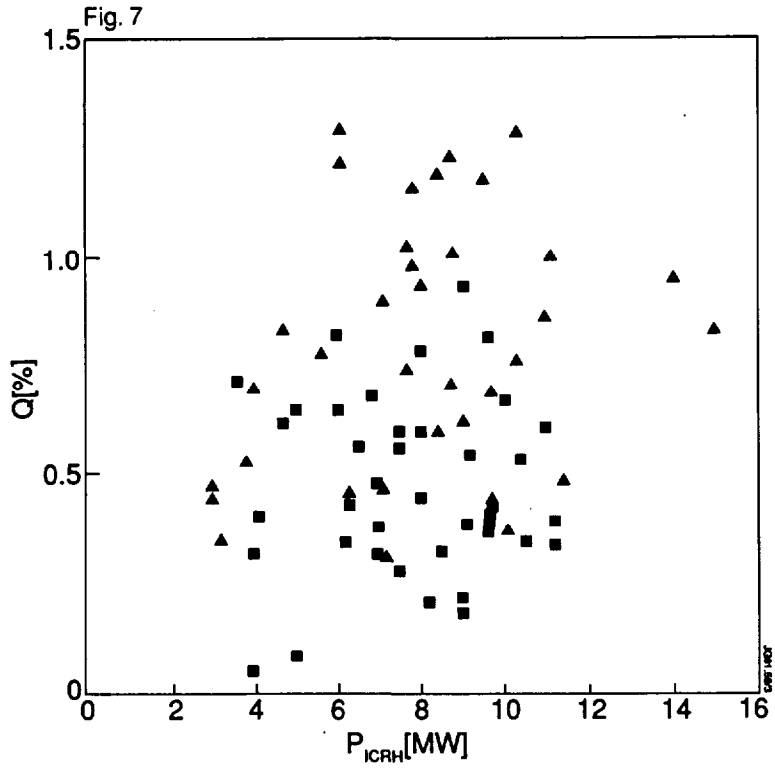

Fig 7: Measured Q as a function of coupled RF power for 3.5 MA discharges with the RF antennas in monopole configuration;
▲ ^{3}He gas puff
■ ^{3}He NBI

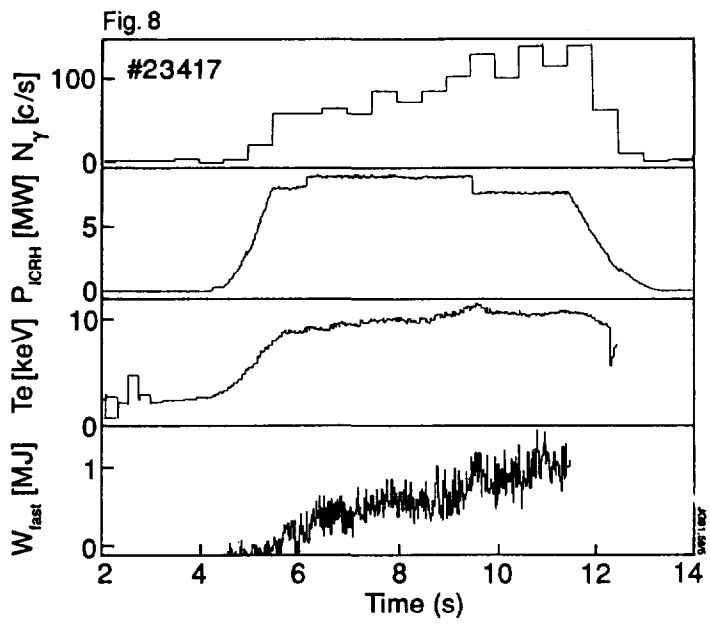

Fig 8: Time evolution of a) D-^{3}He γ-ray emission, b) coupled RF power, c) central electron temperature, and d) perpendicular energy stored in fast particles deduced from magnetic measurements (diamagnetism and plasma equilibrium). Note the correlation between the fusion yield and W_{fast} as predicted by equation 6.

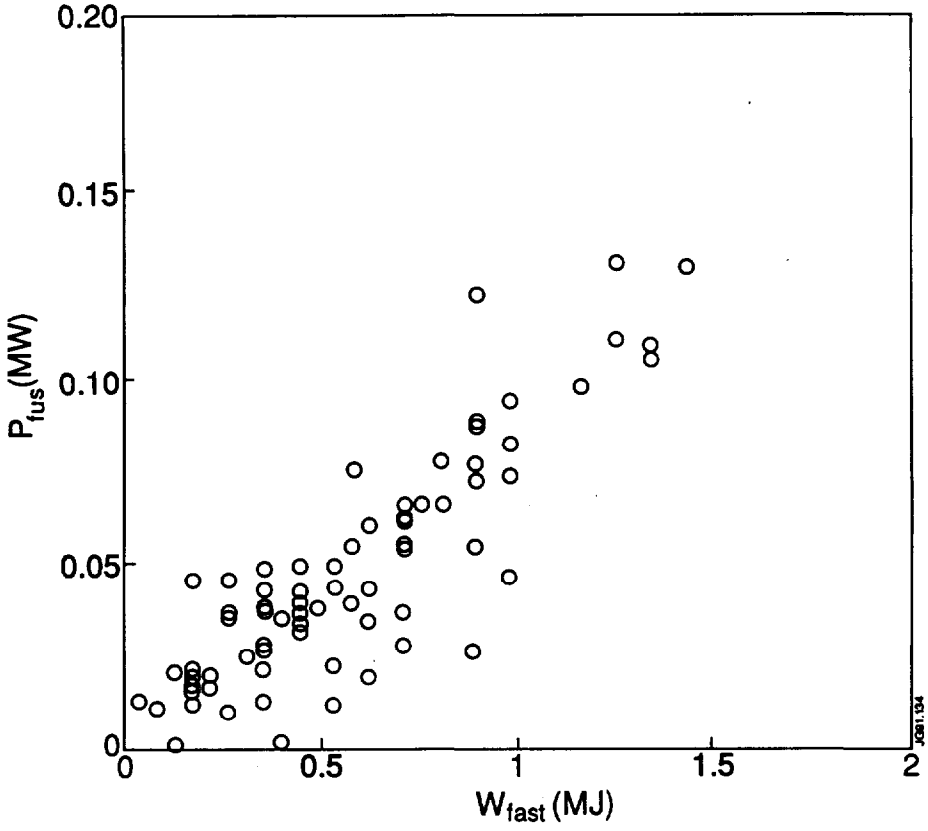

Fig 9: D-^{3}He fusion yield versus the perpendicular energy of the fast ^{3}He ions determined from magnetic measurements (W_{fast} = $4(W_{dia} - w_{MHD})/3$). These results should be compared to the theoretical results of Fig 13.

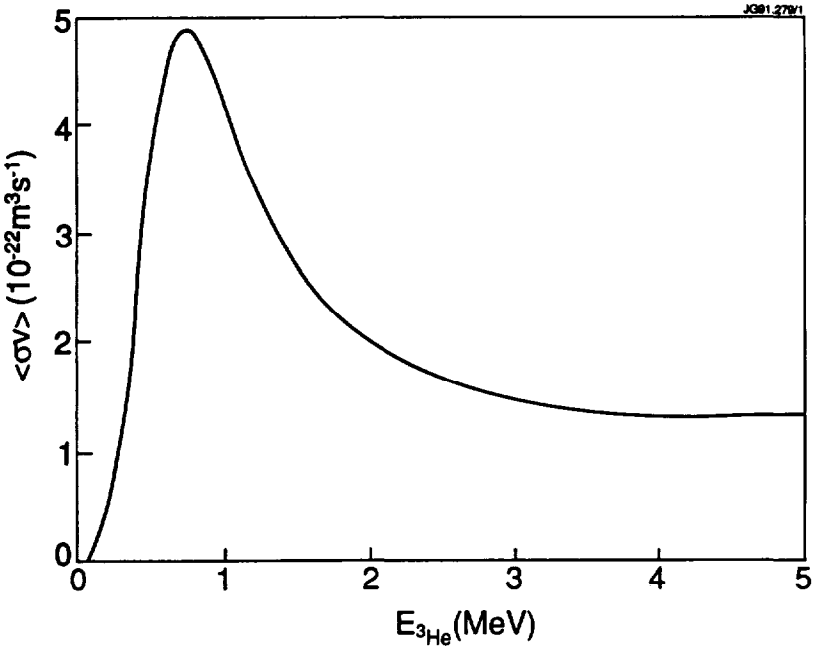

Fig 10: $< \sigma v >$ versus ^{3}He test particle energy calculated from updated cross-sections. The calculation is made for test ^{3}He particles colliding on a maxwellian background deuterium species (T_i = 10 keV).

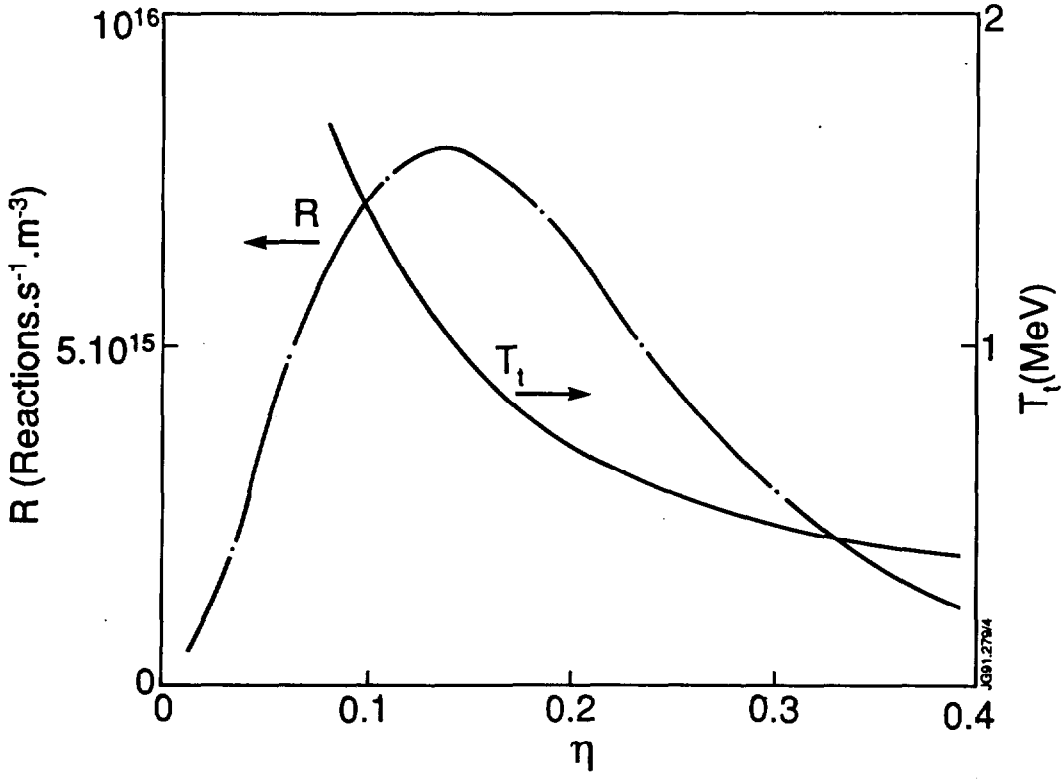

Fig 11: Central values of the fusion reactivity and ^{3}He tail temperature T_t versus $\eta = n_{3He}/n_e$. The optimum conditions corresponds to $T_t \sim 1$ MeV and $\eta \sim 0.12$.

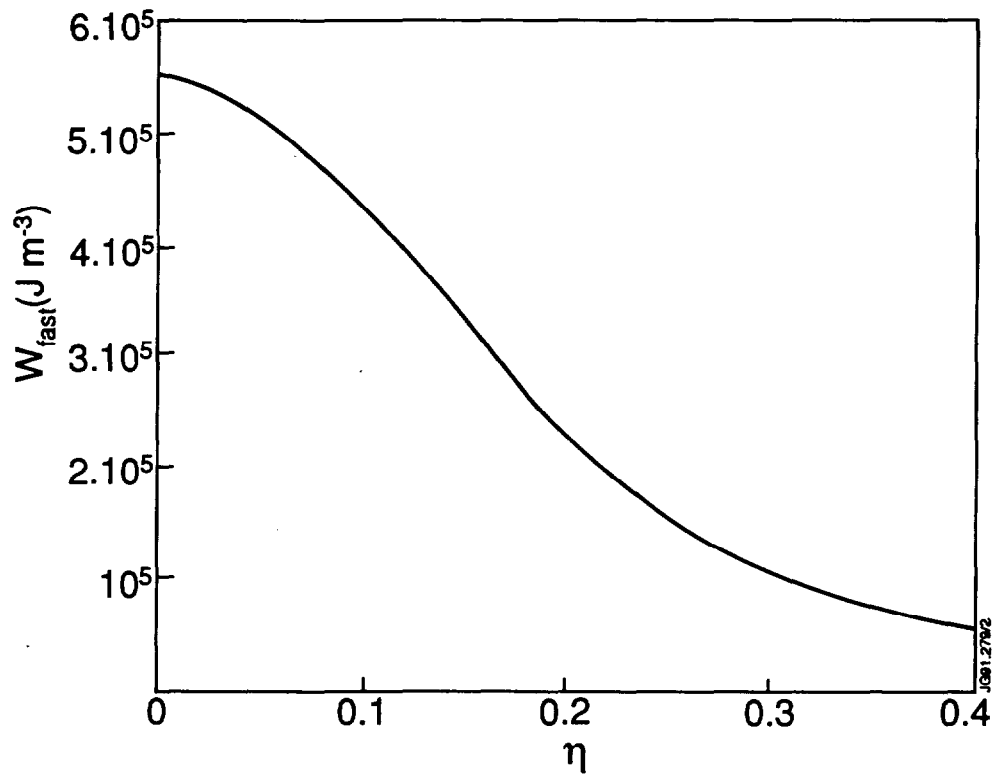

Fig 12: Central value of the fast particle energy density versus η.

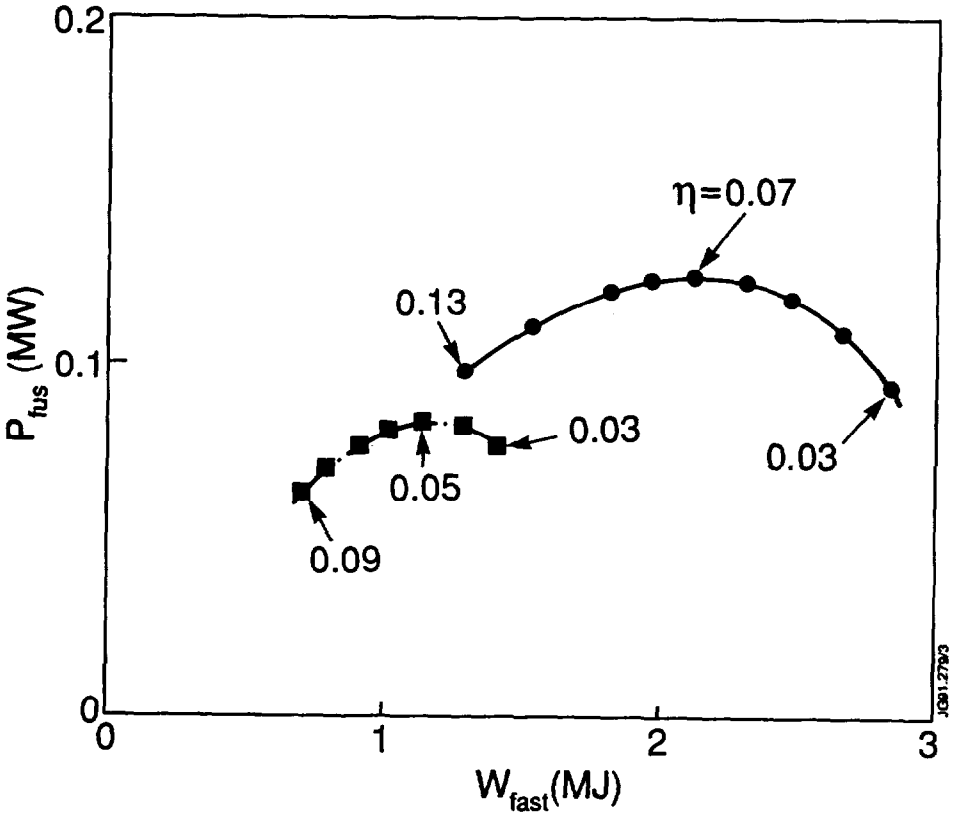

Fig 13: Total fusion output versus W_{fast} from equations 11 and 12. The ^3He concentration η is indicated on the curves. The parameters are given in Table 2 except for: lower curve, T_e = 8 keV, P = 7.5 MW and upper curve T_e = 10 keV, P = 10 MW.

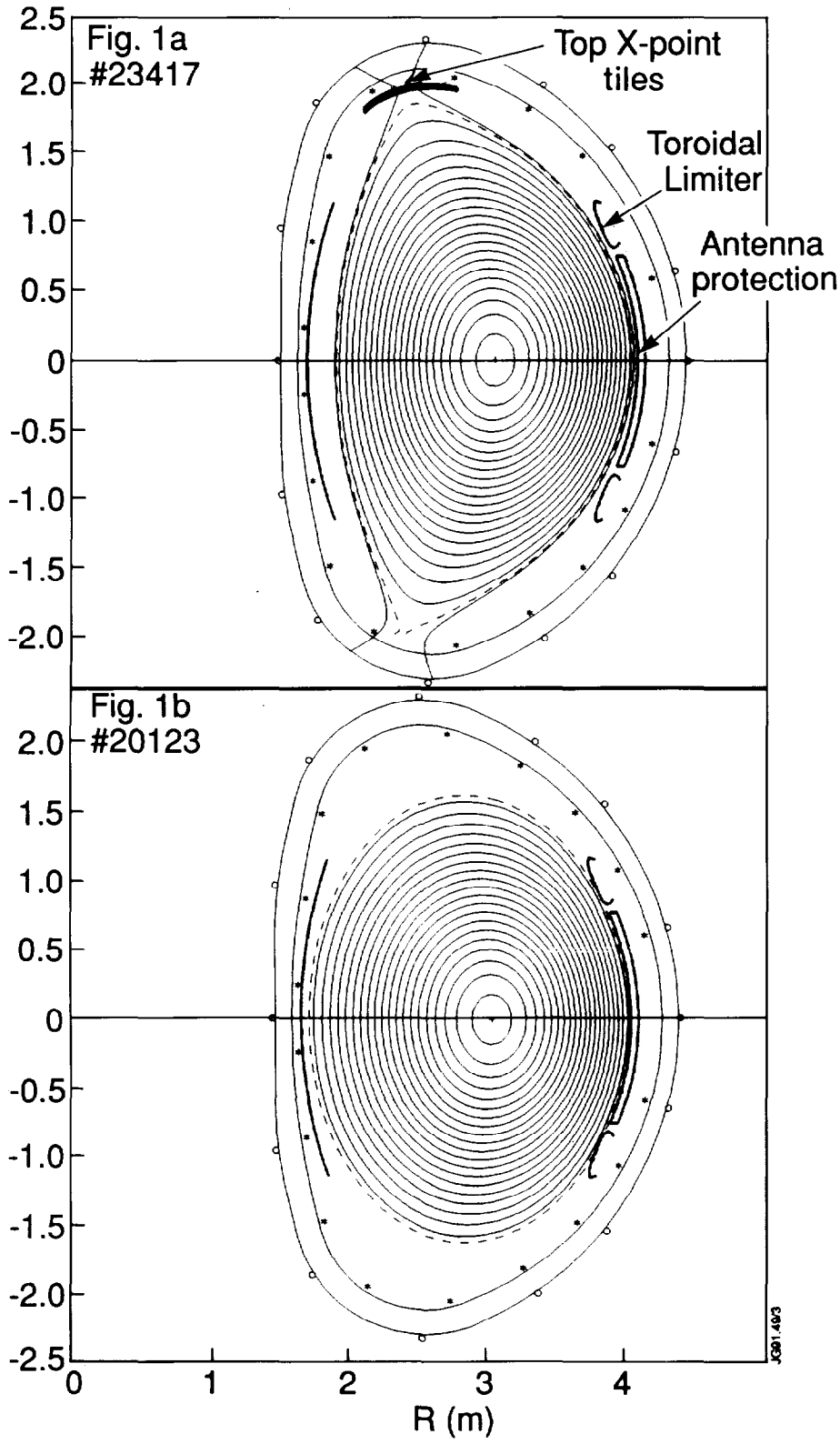

Fig 1: Poloidal flux contours in the plasma used in the series of experiments reported here (Fig 1a) and in a previous series of experiments performed in 1989 (Fib 1b). The points of contact of the last closed surfaces with the limiters are indicated.

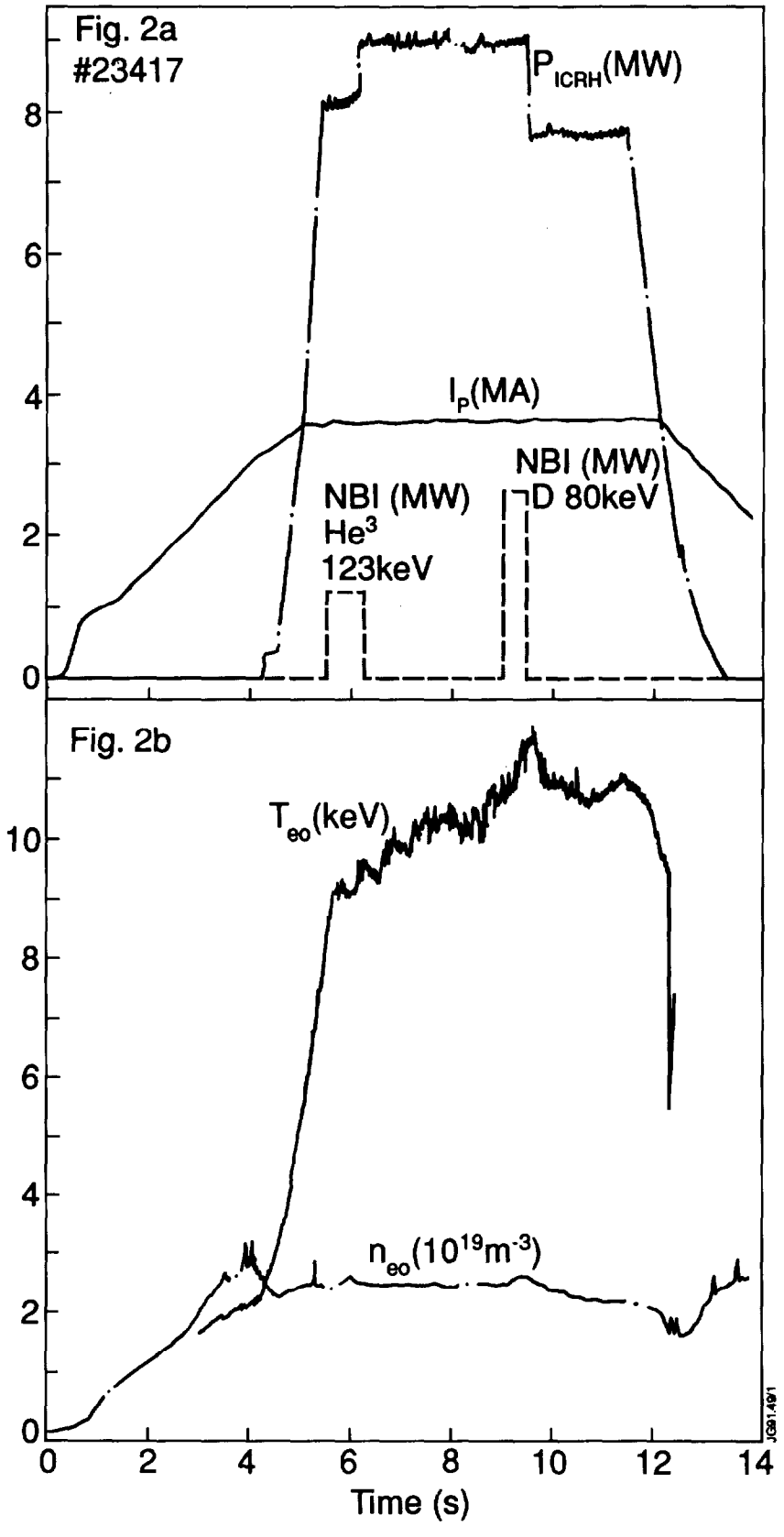

Fig 2: Evolution of the important quantities during a typical high fusion yield experiments: plasma current (I_p), ICRF power, NBI ^{3}He for fuelling and D for charge exchange measurements, central electron temperature (T_{eo}) and density (n_{eo}).

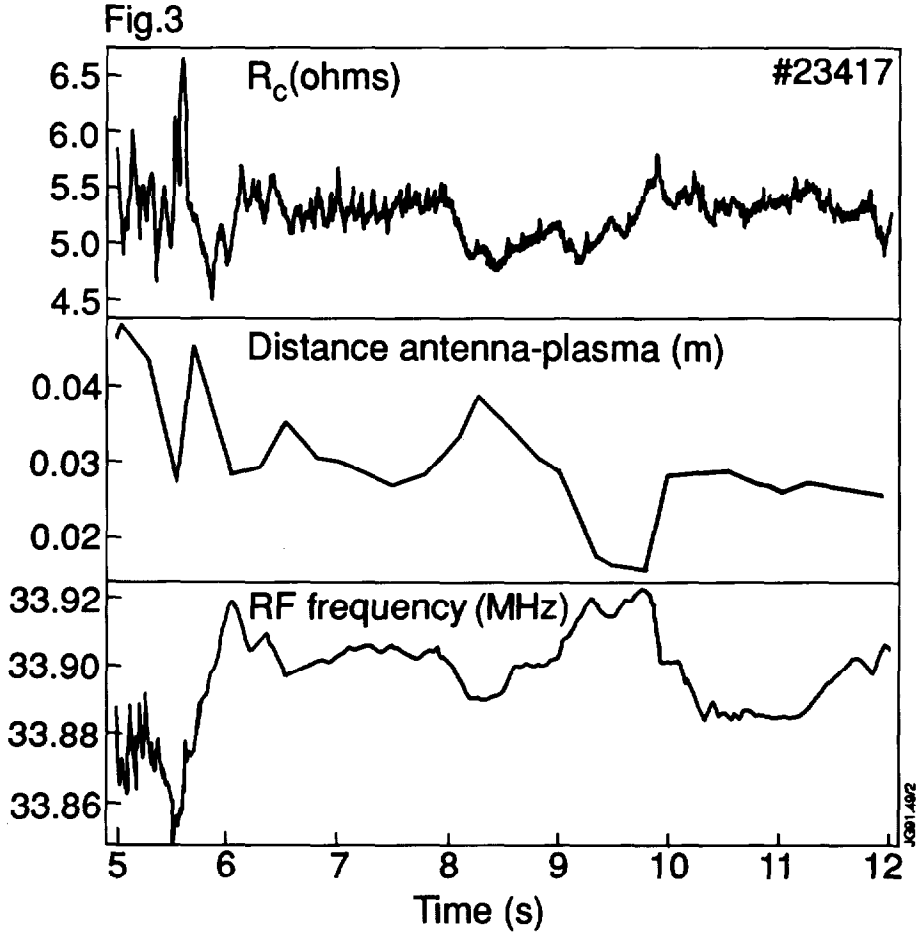

Fig 3: Evolution of the ICRF antenna loading resistance (R_c), the antenna-plasma distance and ICRH frequency. Both the antenna-plasma distance and the RF frequency are under feedback control to maintain constant R_c and the imaginary impedance seen by the generators.

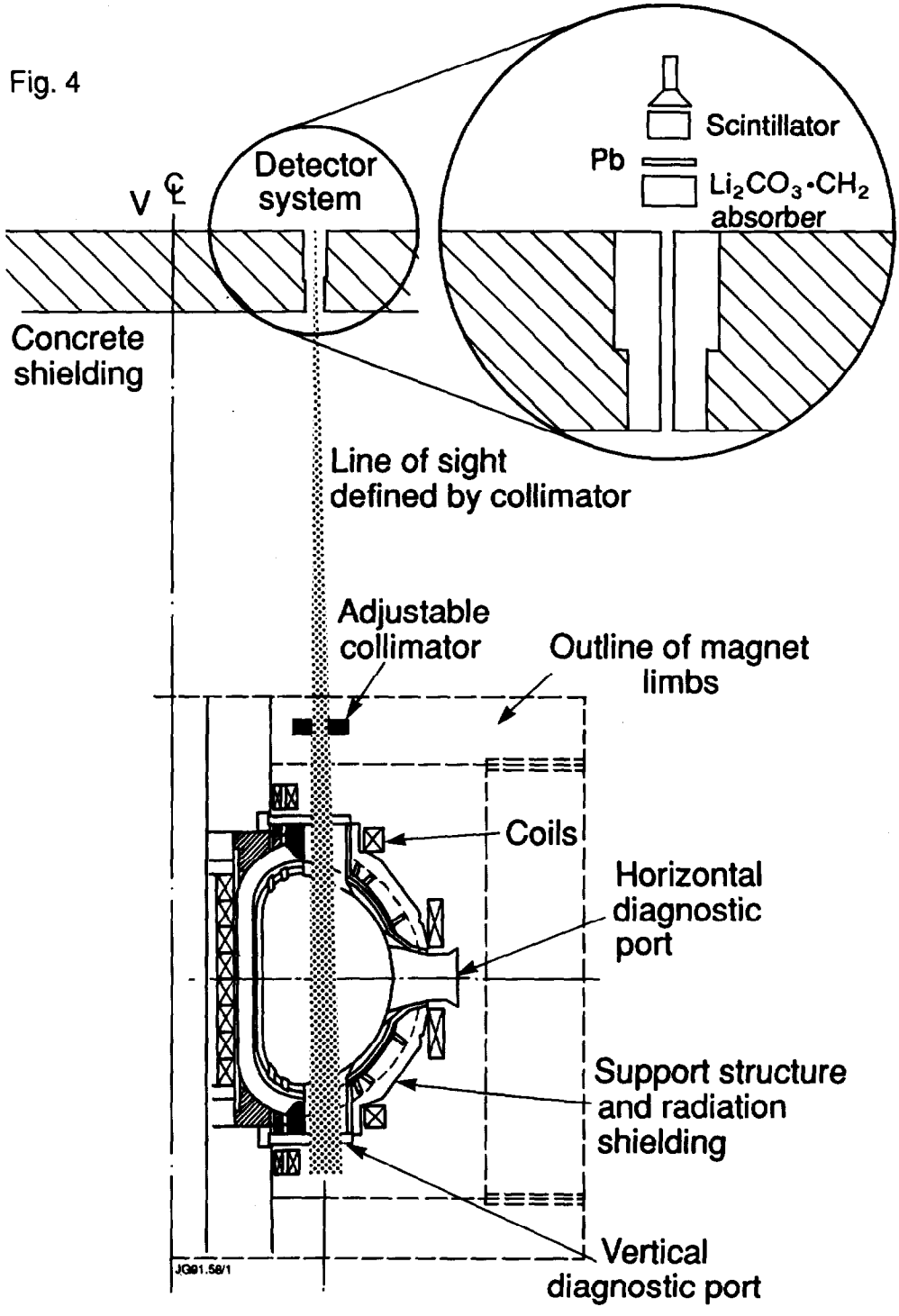

Fig: 4 Experimental arrangement showing one of the two vertical lines-of-sight used in the series of experiment described in the present paper.

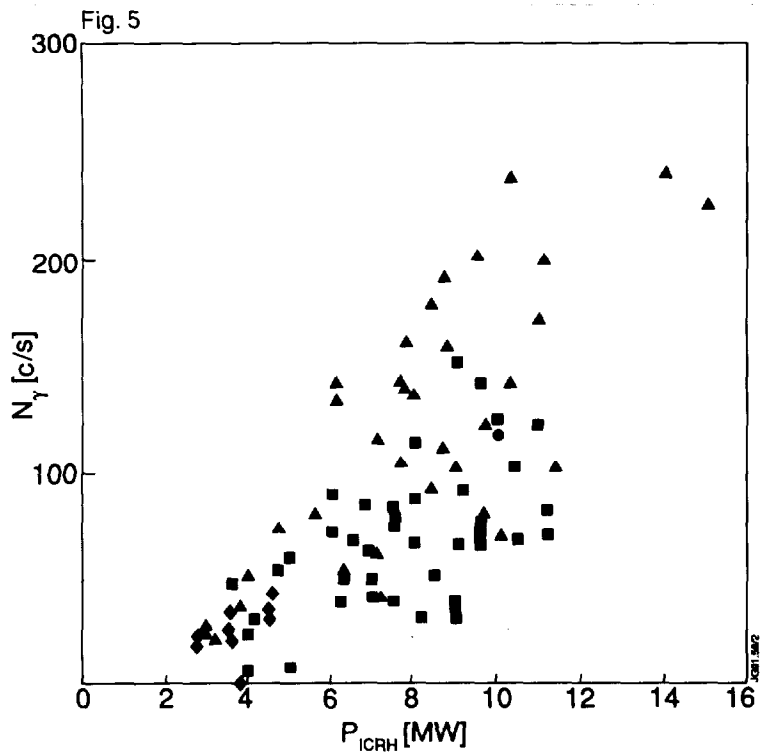

Fig 5: Variation of γ-ray yield as a function of coupled RF power;
▲ ^{3}He gas puff, monopole configuration, 3.5 MA
■ ^{3}He NBI, monopole configuration, 3.5 MA
◆ ^{3}He gas puff and/or ^{3}He NBI, dipole configuration, 3.5 MA
● ^{3}He gas puff, monopole configuration, 5 MA

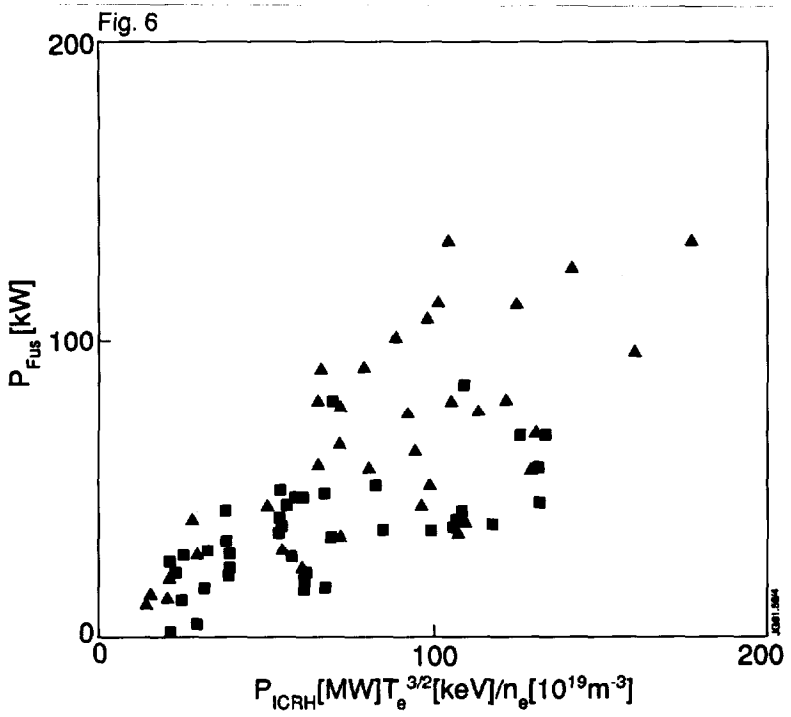

Fig 6: D-^{3}He Fusion Power as a function of P_{ICRH} $T_e^{3/2}$ $n_e \propto W_{fast}$ for 3.5 MA discharges;
▲ ^{3}He gas puff
■ ^{3}He NBI

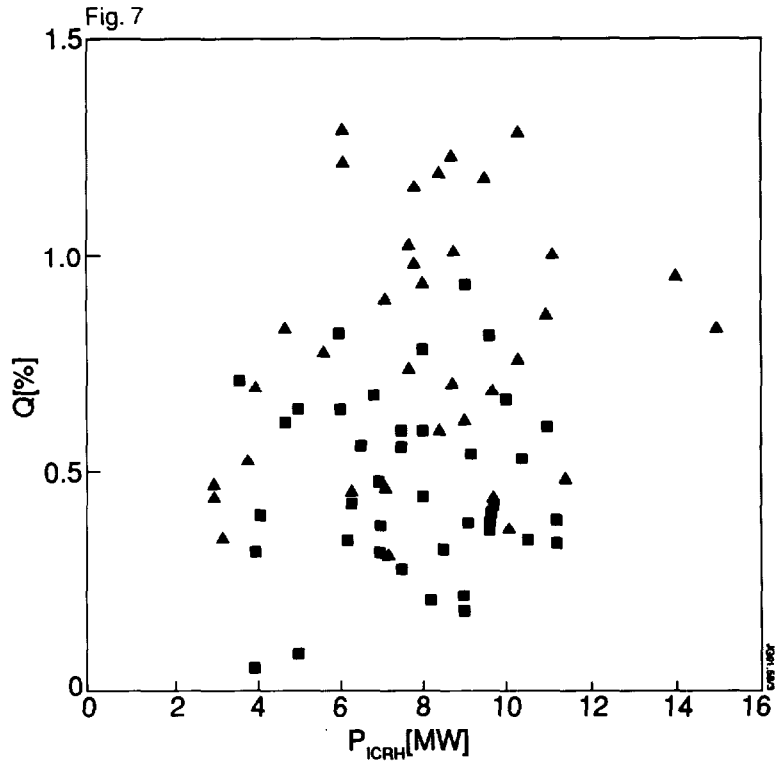

Fig 7: Measured Q as a function of coupled RF power for 3.5 MA discharges with the RF antennas in monopole configuration;
▲ ^{3}He gas puff
■ ^{3}He NBI

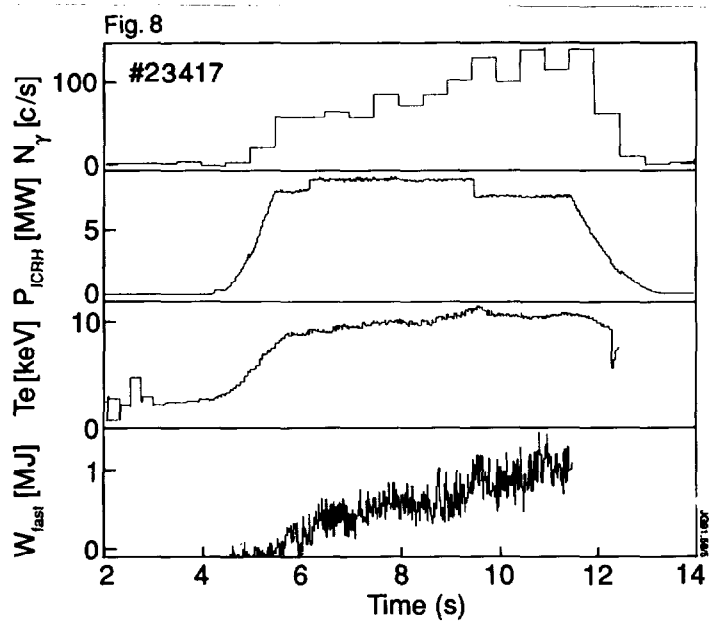

Fig 8: Time evolution of a) D-^{3}He γ-ray emission, b) coupled RF power, c) central electron temperature, and d) perpendicular energy stored in fast particles deduced from magnetic measurements (diamagnetism and plasma equilibrium). Note the correlation between the fusion yield and W_{fast} as predicted by equation 6.

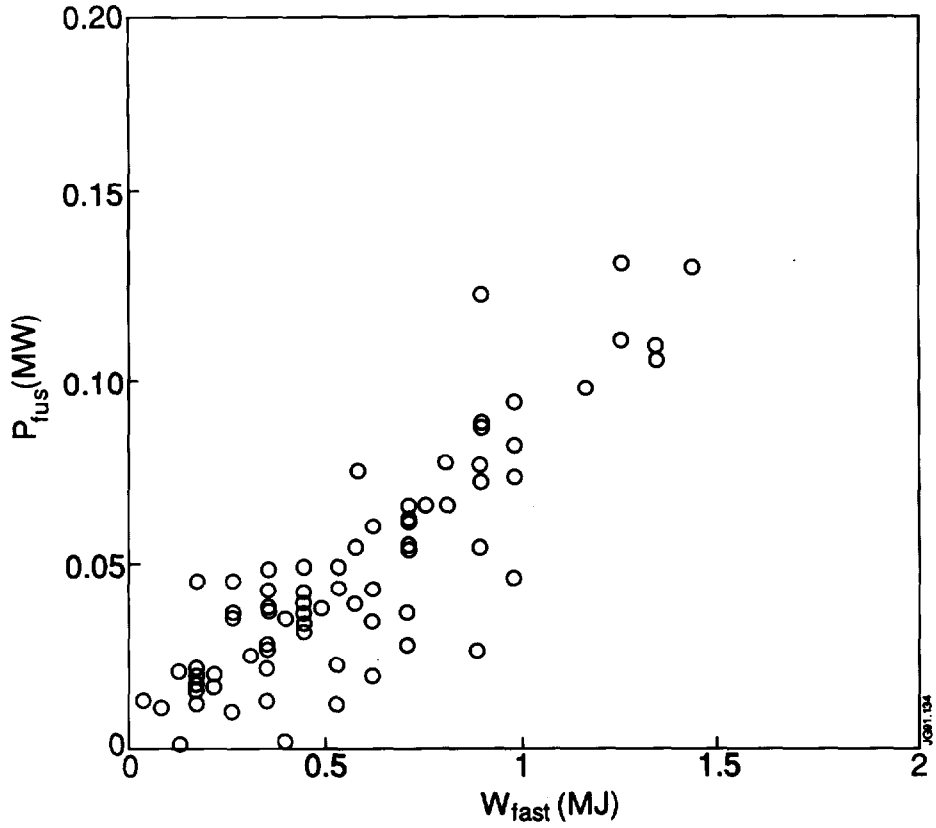

Fig 9: D-^{3}He fusion yield versus the perpendicular energy of the fast ^{3}He ions determined from magnetic measurements (W_{fast} = $4(W_{dia} - w_{MHD})/3$). These results should be compared to the theoretical results of Fig 13.

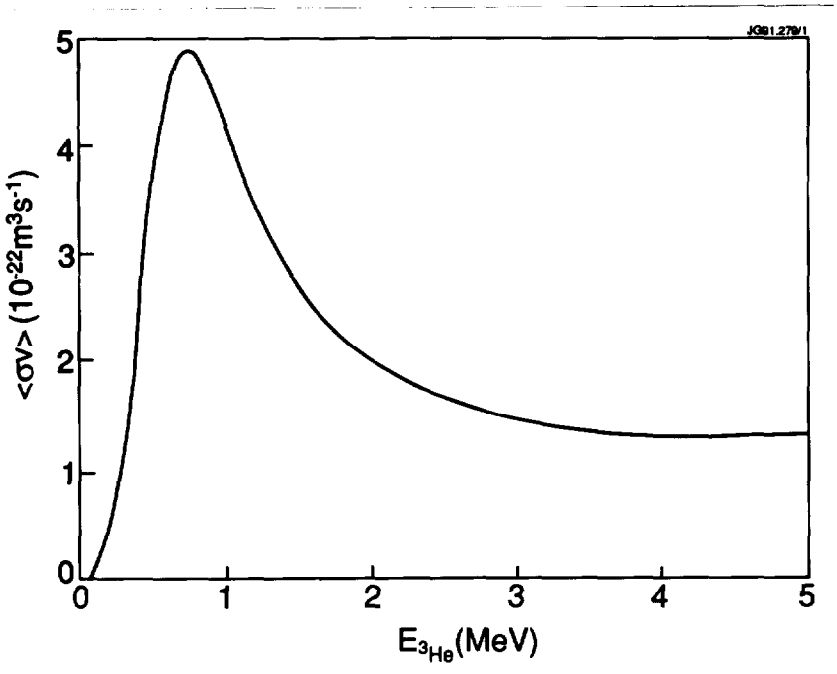

Fig 10: $< \sigma v >$ versus ^{3}He test particle energy calculated from updated cross-sections. The calculation is made for test ^{3}He particles colliding on a maxwellian background deuterium species (T_i = 10 keV).

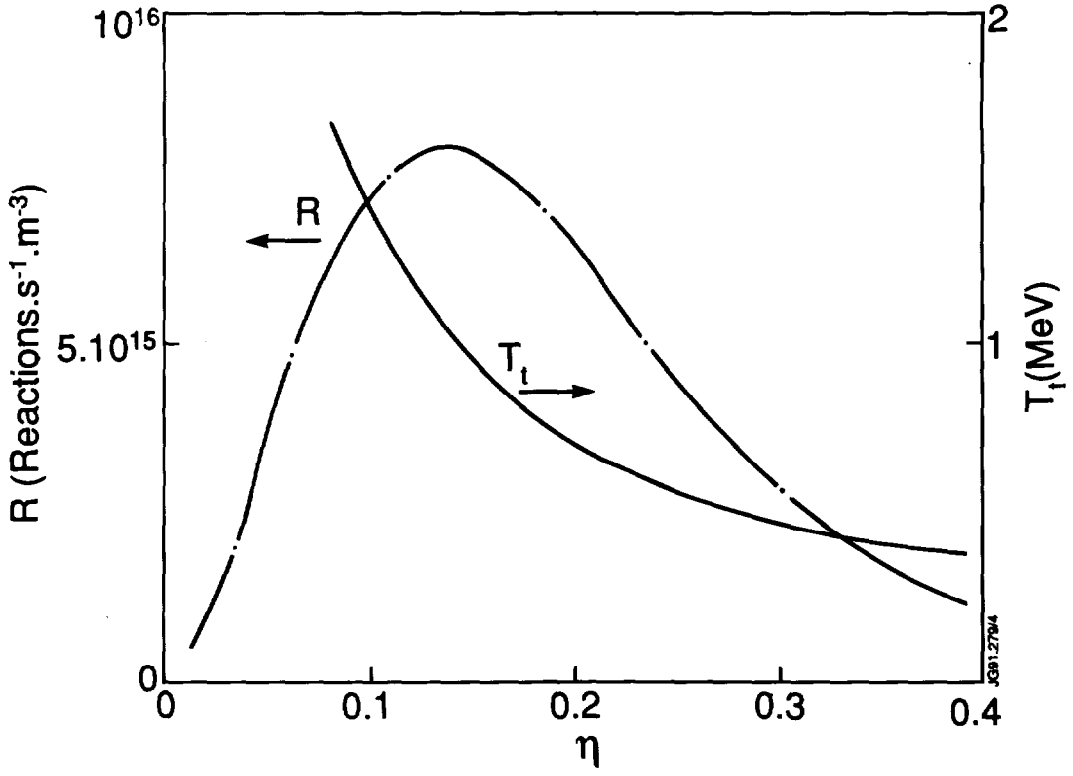

Fig 11: Central values of the fusion reactivity and ^{3}He tail temperature T_t versus $\eta = n_{3He}/n_e$. The optimum conditions corresponds to $T_t \sim 1$ MeV and $\eta \sim 0.12$.

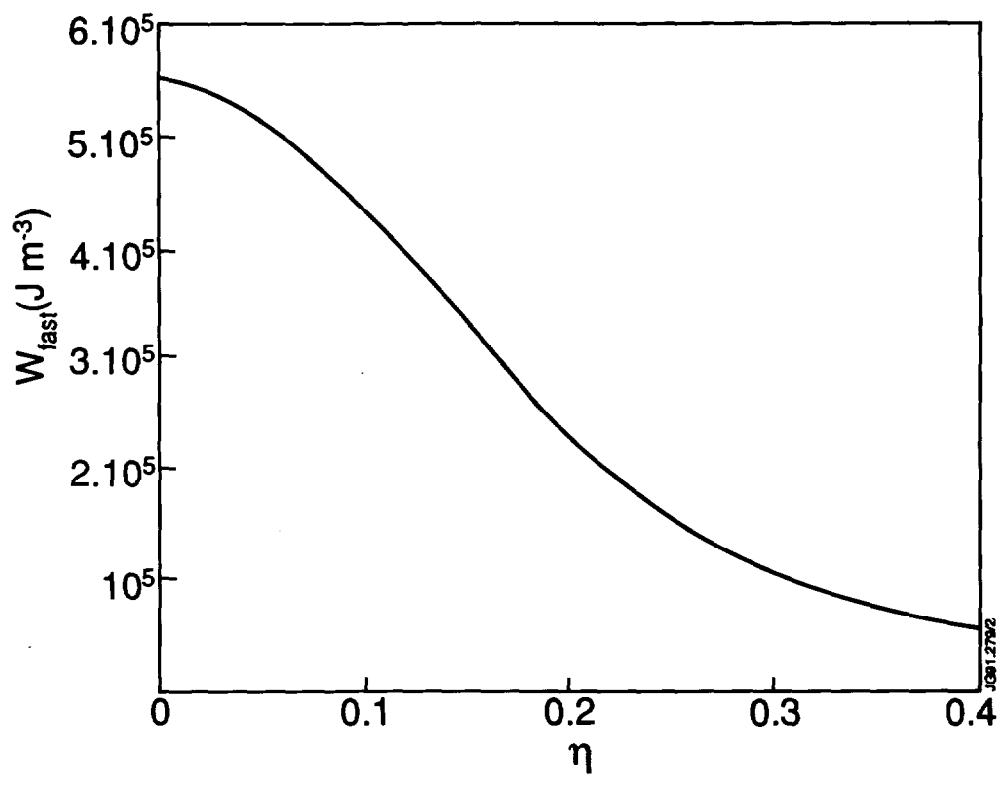

Fig 12: Central value of the fast particle energy density versus η.

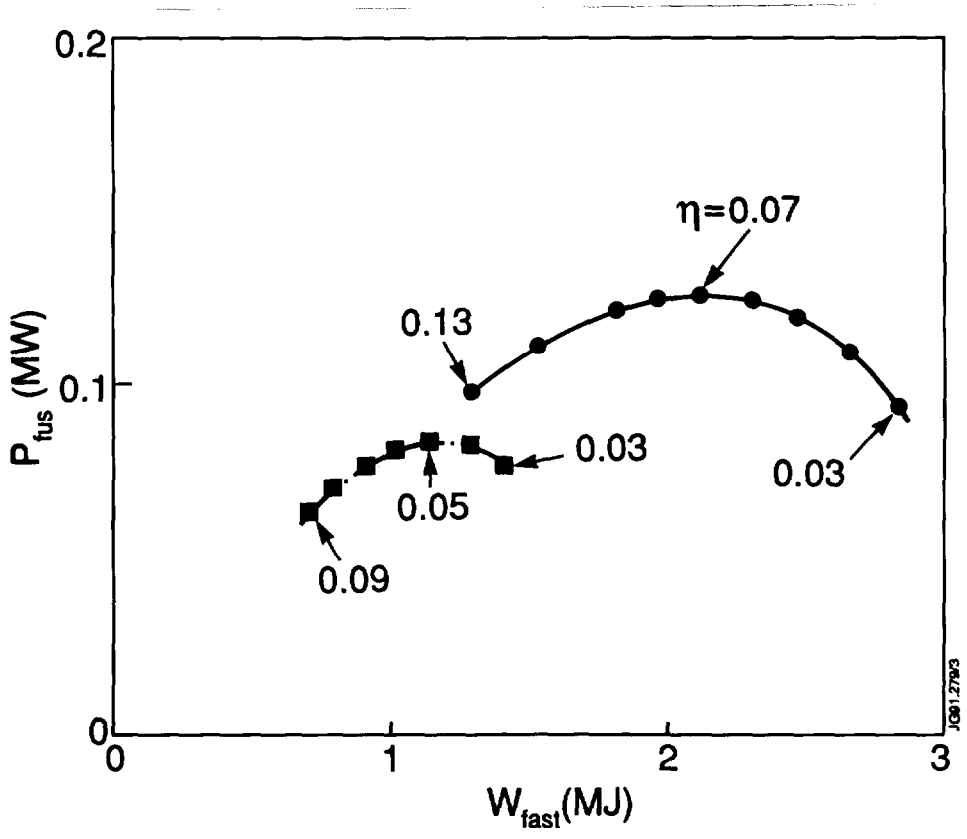

Fig 13: Total fusion output versus W_{fast} from equations 11 and 12. The ^3He concentration η is indicated on the curves. The parameters are given in Table 2 except for: lower curve, T_e = 8 keV, P = 7.5 MW and upper curve T_e = 10 keV, P = 10 MW.

APPENDIX 1.

THE JET TEAM

JET Joint Undertaking, Abingdon, Oxon, OX14 3EA, U.K.

J.M.Adams[1], F.Alladio[4], H.Altmann, R.J.Anderson, G.Appruzzese, W.Bailey, B.Balet, D.V.Bartlett, L.R.Baylor[24], K.Behringer, A.C.Bell, P.Bertoldi, E.Bertolini, V.Bhatnagar, R.J.Bickerton, A.Boileau[3], T.Bonicelli, S.J.Booth, G.Bosia, M.Botman, D.Boyd[31], H.Brelen, H.Brinkschulte, M.Brusati, T.Budd, M.Bures, T.Businaro[4], H.Buttgereit, D.Cacaut, C.Caldwell-Nichols, D.J.Campbell, P.Card, J.Carwardine, G.Celentano, P.Chabert[27], C.D.Challis, A.Cheetham, J.Christiansen, C.Christodoulopoulos, P.Chuilon, R.Claesen, S.Clement[30], J.P.Coad, P.Colestock[6], S.Conroy[13], M.Cooke, S.Cooper, J.G.Cordey, W.Core, S.Corti, A.E.Costley, G.Cottrell, M.Cox[7], P.Cripwell[13], F.Crisanti[4], D.Cross, H.de Blank[16], J.de Haas[16], L.de Kock, E.Deksnis, G.B.Denne, G.Deschamps, G.Devillars, K.J.Dietz, J.Dobbing, S.E.Dorling, P.G.Doyle, D.F.Düchs, H.Duquenoy, A.Edwards, J.Ehrenberg[14], T.Elevant[12], W.Engelhardt, S.K.Erents[7], L.G.Eriksonn[5], M.Evrard[2], H.Falter, D.Flory, M.Forrest[7], C.Froger, K.Fullard, M.Gadeberg[11], A.Galetsas, R.Galvao[8], A.Gibson, R.D.Gill, A.Gondhalekar, C.Gordon, G.Gorini, C.Gormezano, N.A.Gottardi, C.Gowers, B.J.Green, F.S.Griph, M.Gryzinski[26], R.Haange, G.Hammett[6], W.Han[9], C.J.Hancock, P.J.Harbour, N.C.Hawkes[7], P.Haynes[7], T.Hellsten, J.L.Hemmerich, R.Hemsworth, R.F.Herzog, K.Hirsch[14], J.Hoekzema, W.A.Houlberg[24], J.How, M.Huart, A.Hubbard, T.P.Hughes[32], M.Hugon, M.Huguet, J.Jacquinot, O.N.Jarvis, T.C.Jernigan[24], E.Joffrin, E.M.Jones, L.P.D.F.Jones, T.T.C.Jones, J.Källne, A.Kaye, B.E.Keen, M.Keilhacker, G.J.Kelly, A.Khare[15], S.Knowlton, A.Konstantellos, M.Kovanen[21], P.Kupschus, P.Lallia, J.R.Last, L.Lauro-Taroni, M.Laux[33], K.Lawson[7], E.Lazzaro, M.Lennholm, X.Litaudon, P.Lomas, M.Lorentz-Gottardi[2], C.Lowry, G.Magyar, D.Maisonnier, M.Malacarne, V.Marchese, P.Massmann, L.McCarthy[28], G.McCracken[7], P.Mendonca, P.Meriguet, P.Micozzi[4], S.F.Mills, P.Millward, S.L.Milora[24], A.Moissonnier, P.L.Mondino, D.Moreau[17], P.Morgan, H.Morsi[14], G.Murphy, M.F.Nave, M.Newman, L.Nickesson, P.Nielsen, P.Noll, W.Obert, D.O'Brien, J.O'Rourke, M.G.Pacco-Düchs, M.Pain, S.Papastergiou, D.Pasini[20], M.Paume[27], N.Peacock[7], D.Pearson[13], F.Pegoraro, M.Pick, S.Pitcher[7], J.Plancoulaine, J-P.Poffé, F.Porcelli, R.Prentice, T.Raimondi, J.Ramette[17], J.M.Rax[27], C.Raymond, P-H.Rebut, J.Removille, F.Rimini, D.Robinson[7], A.Rolfe, R.T.Ross, L.Rossi, G.Rupprecht[14], R.Rushton, P.Rutter, H.C.Sack, G.Sadler, N.Salmon[13], H.Salzmann[14], A.Santagiustina, D.Schissel[25], P.H.Schild, M.Schmid, G.Schmidt[6], R.L.Shaw, A.Sibley, R.Simonini, J.Sips[16], P.Smeulders, J.Snipes, S.Sommers, L.Sonnerup, K.Sonnenberg, M.Stamp, P.Stangeby[19], D.Start, C.A.Steed, D.Stork, P.E.Stott, T.E.Stringer, D.Stubberfield, T.Sugie[18], D.Summers, H.Summers[20], J.Taboda-Duarte[22], J.Tagle[30], H.Tamnen, A.Tanga, A.Taroni, C.Tebaldi[23], A.Tesini, P.R.Thomas, E.Thompson, K.Thomsen[11], P.Trevalion, M.Tschudin, B.Tubbing, K.Uchino[29], E.Usselmann, H.van der Beken, M.von Hellermann, T.Wade, C.Walker, B.A.Wallander, M.Walravens, K.Walter, D.Ward, M.L.Watkins, J.Wesson, D.H.Wheeler, J.Wilks, U.Willen[12], D.Wilson, T.Winkel, C.Woodward, M.Wykes, I.D.Young, L.Zannelli, M.Zarnstorff[6], D.Zasche[14], J.W.Zwart.

PERMANENT ADDRESS

1. UKAEA, Harwell, Oxon. UK.
2. EUR-EB Association, LPP-ERM/KMS, B-1040 Brussels, Belgium.
3. Institute National des Récherches Scientifique, Quebec, Canada.
4. ENEA-CENTRO Di Frascati, I-00044 Frascati, Roma, Italy.
5. Chalmers University of Technology, Göteborg, Sweden.
6. Princeton Plasma Physics Laboratory, New Jersey, USA.
7. UKAEA Culham Laboratory, Abingdon, Oxon. UK.
8. Plasma Physics Laboratory, Space Research Institute, Sao José dos Campos, Brazil.
9. Institute of Mathematics, University of Oxford, UK.
10. CRPP/EPFL, 21 Avenue des Bains, CH-1007 Lausanne, Switzerland.
11. Risø National Laboratory, DK-4000 Roskilde, Denmark.
12. Swedish Energy Research Commission, S-10072 Stockholm, Sweden.
13. Imperial College of Science and Technology, University of London, UK.
14. Max Planck Institut für Plasmaphysik, D-8046 Garching bei München, FRG.
15. Institute for Plasma Research, Gandhinagar Bhat Gujat, India.
16. FOM Instituut voor Plasmafysica, 3430 Be Nieuwegein, The Netherlands.
17. Commissiariat à L'Energie Atomique, F-92260 Fontenay-aux-Roses, France.
18. JAERI, Tokai Research Establishment, Tokai-Mura, Naka-Gun, Japan.
19. Institute for Aerospace Studies, University of Toronto, Downsview, Ontario, Canada.
20. University of Strathclyde, Glasgow, G4 ONG, U.K.
21. Nuclear Engineering Laboratory, Lapeenranta University, Finland.
22. JNICT, Lisboa, Portugal.
23. Department of Mathematics, Univeristy of Bologna, Italy.
24. Oak Ridge National Laboratory, Oak Ridge, Tenn., USA.
25. G.A. Technologies, San Diego, California, USA.
26. Institute for Nuclear Studies, Swierk, Poland.
27. Commissiariat à l'Energie Atomique, Cadarache, France.
28. School of Physical Sciences, Flinders University of South Australia, South Australia SO42.
29. Kyushi University, Kasagu Fukuoka, Japan.
30. Centro de Investigaciones Energeticas Medioambientales y Techalogicas, Spain.
31. University of Maryland, College Park, Maryland, USA.
32. University of Essex, Colchester, UK.
33. Akademie de Wissenschaften, Berlin, DDR.

CR 88.49.1A